ACADEMIC PRESS

Available online at www.sciencedirect.com

SCIENCE DIRECT®

Journal of Sound and Vibration 263 (2003) 743–774

JOURNAL OF SOUND AND VIBRATION

www.elsevier.com/locate/jsvi

On the dragged surge vibration of twin TLP systems with multi-interactions of wave and structures

Hsien Hua Lee*, Wen-Sheng Wang

Department of Marine Environment and Engineering, National Sun Yat-sen University, Kaohsiung, Taiwan

Received 4 July 2000; accepted 8 July 2002

Abstract

In this study, the wave-induced surge motion of a twin platform of tension leg structural system was investigated. A set of equations along with boundary conditions was derived, and solutions were obtained analytically. In the analysis the coupling problem of a two-dimensional tension leg twin platform interacting with a monochromatic linear wave train in an inviscid and incompressible fluid is considered. The problem was considered as a combination of the scattering and radiation problem. These two boundary-value problems were first solved independently and then combined together to resolve for all unknowns. The analysis was focused on the wave-induced surge motion of the twin platform and the reflection coefficient when the multi-interactions among waves, platform structure and the tension legs were taken into account. From the analytical results, it was found that ignoring the interaction effect between the tether and waves for a twin platform system, it tends to overestimate the wave-induced response in general. It was also realized that the behavior of the tension-leg twin platform was significantly influenced by dimensional factors of the platform system such as the dimension of each platform and the spacing between two platforms.

1. Introduction

Tension-leg platforms (TLPs) are usually used as working station for oil exploration in deep water. Lately, the application on this structural system is even wider such as the floating breakwater system and the fish-farming cage system. The TLPs are constituted of a semi-submerged structure (pontoon) and pre-tensioned tethers anchored to the ocean bed. The difficulty in the dynamic analysis of the TLPs is due to the non-linearity of the TLP motion and

*Corresponding author. Tel.: +886-7-525-2000x5069; fax: +886-7-525-5060.
E-mail address: hhlee@mail.nsysu.edu.tw (H.H. Lee).

0022-460X/03/$ - see front matter
PII: S0022-460X(02)01108-2

the boundary conditions on the free surface and on the structural bottom [1]. For this problem the linear boundary-value problem is incorporated into a scattering problem and a radiation problem [2]. This problem was solved by a numerical method since 1970s [3,4], and also studied in experimental test [4]. An analytical solution was proposed later and demonstrated by Lee and Lee [5], where the surge motion of a single platform with pre-tensioned tethers was calculated.

In that study, however, the elasticity of tethers was only implied and the motion of tethers was also simplified as on-line rigid-body motion proportional to the top platform. Thus, both the material property and the mechanical behavior for the tether incorporated in the TLP system were ignored. When this simplification was applied, no matter what material was used or what the dimension of the tethers was, the dynamic response of the platform would remain the same in terms of the vibration mode, periods and the vibration amplitude. This is not true for the actual engineering application. Therefore, in a more recent study [6], both the property and the dimension of the tether material were considered and the equation of motion was modified with the corresponding material parameters. The results showed that the dynamic behavior of both the tether of TLP and the platform itself is closely related to the material property and the tether dimension while the influence of wave properties remains constant.

In the actual engineering application a twin platform system is more practical such as platforms with two separate pontoons or similar devices under the deck, however, most analyses aforementioned concentrated on the traditional single-platform system. Even though a twin-platform system might be simplified into a single-platform system, the analytical results are greatly subjected to the dimensional influence of the platform structural system. The determination of the dimensional parameters could affect the platform behavior and how a twin-platform system could be simplified by a single-platform solution. For the problems of a tension-leg twin-platform structural system, the analytical solutions without considering the interactions between wave and tension legs were obtained lately [7]. In that study some parameter effects on the surge motion were also discussed. However, for more realistic engineering practice, solutions accounting for the multi-interactions among waves, platform structure and the tension-leg tethers will be necessary. Therefore, it is the purpose of this study to find an appropriate method that may more accurately describe the behavior of the tension-leg twin-platform structural system when subjected to the multi-interactions among waves, platform and tension-leg tethers. Furthermore, the factors that may influence the behavior of this twin-platform system such as the platform spacing, platform dimensions and water-related properties are all under consideration for the analysis.

Generally a 2-D approach was applied to simulate a 3-D TLP problem [4] even though the 3-D system was practiced. However, for a platform system with an obvious larger third dimension such as a long floating breakwaters or multi-purpose platforms, the wave incident normal to the long axis will be the concern while the behavior in the third direction is much less important. Thus a 2-D approach will be appropriate to simulate the motion of this 3-D system. In this study, based on previous works [5–8] a set of equations and corresponding boundary conditions were derived and then solved analytically. These equations were combined into the equation of motion for the tether and the equation for the platform motion and then solved simultaneously to obtain the flow field, platform responses and the tether motion. The material properties of tethers were taken into account and the region of water was separated into five parts according to the actual twin-platform geometry. The analysis was focused on the reflection coefficient and the wave-induced

drag surge motion of the platform. The comparison was also made for the platform motion between the twin-platform system with and without accounting for the tether–wave interactions. In addition to the wave-related parameters, the dimensional effect of the twin-platform structure was examined and presented in numerical examples. From the analytical results, it was found that the behavior of the tension-leg twin-platform system was not only significantly influenced by the dimensional parameters of the platform such as the dimension of each single platform and the spacing between two platforms but also by the tether–wave interactions. It was also realized from the numerical results that similar to the single-platform case [8], the interaction of tether and waves reduces the platform motion to a great deal. When the twin-platform is located in deep water or the platform has a shallow draft or small dimension, the engineering design and calculation without considering the tether–wave interaction effect may significantly overestimate the platform responses. Additionally, a phenomenon similar to the water oscillations in a basin was also studied for this twin-platform structural system as incident waves reflect in between two platforms of the system. It was observed that the drags induced from the interaction effect of the twin-platform structural system could also influence the water oscillations between the platforms.

2. General wave theory

For the inviscid and incompressible fluid and irrotational flow, a single-valued velocity potential ϕ can be defined as

$$u = -\nabla\phi, \tag{1}$$

where u is the velocity potential and ∇ is the gradient operator. The velocity potential satisfies the Laplace equation

$$\nabla^2\phi = 0 \tag{2}$$

and the Bernoulli equation in the flow field as

$$-\frac{\partial\phi}{\partial t} + \frac{1}{2}\nabla\phi\nabla\phi + \frac{p}{\rho_w} + gz = 0, \tag{3}$$

where p is the pressure, ρ_w the water density, g the gravitational constant, and z the water depth. The non-linear term in Eq. (3) can be ignored when we deal with linear small amplitude wave, and assume that the wave height is small compared to the wavelength and water depth.

A 2-D tension-leg twin-platform system interacting with a monochromatic small amplitude wave propagating in the $+x$ direction was considered here as shown in Fig. 1. The waveform and the associated velocity potential are given accordingly as

$$\eta_{Is} = -\mathrm{i}A_i\mathrm{e}^{-(K_1x+\mathrm{i}\sigma t)} \tag{4}$$

and

$$\phi_i = \frac{A_i g}{\sigma}\frac{\cos[K_1(z+h)]}{\cos(K_1h)}\mathrm{e}^{-(K_1x+\mathrm{i}\sigma t)}, \tag{5}$$

where A_i is the wave amplitude, g is the gravitational constant and h is the water depth. $\sigma = 2\pi/T$ is the angular frequency with period T. $K_1 = -\mathrm{i}k$ and $k = 2\pi/L$ is the wave number with

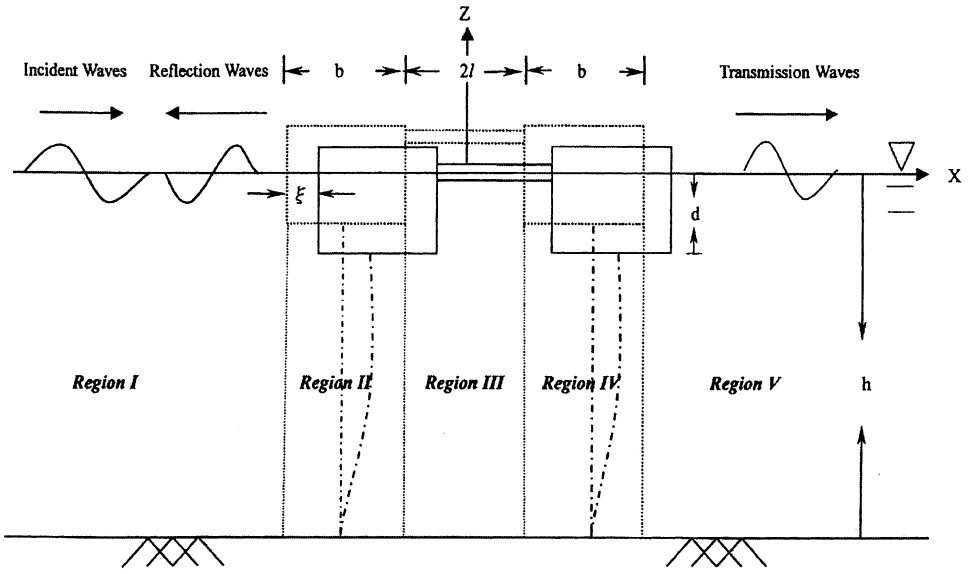

Fig. 1. Illustration for the problem of the tension leg twin-platform system.

wavelength L. K_1 satisfies the dispersion relation given by

$$\sigma^2 = gK_1 \tan(K_1 h). \tag{6}$$

3. Tension-leg twin-platform system

In the platform system, the motion of the structure induced by the small amplitude incident wave is assumed to be small. The wave-induced structural motion can be solved from the imposed boundary problem. Due to the linearity of the problem, the problem can be incorporated into a scattering and a radiation problem [9]. The wave force calculated from the scattering problem provides the force function in the radiation problem, and the forced oscillation then generates outgoing waves.

As is shown in Fig. 1, two platforms (or two single pontoons submerged under the platform) were connected by a member of rigid body in between and the whole flow field under the twin platform system was divided into five regions by four artificial boundaries at $x = -1 - b, -1, +l$ and $l + b$. In region I, $-\infty < x < -l - b$, the total velocity potential ϕ_{I} consists of velocity potentials of incident waves ϕ_i, scattered waves ϕ_{Is} and radiated waves ϕ_{Iw}. In the other regions the total velocity potential consists of velocity potentials of scattered waves and radiated waves such as in region II, $-l - b < x < -l$, ϕ_{II} consists of $\phi_{\mathrm{II}s}$ and $\phi_{\mathrm{II}w}$, in region III, $-l < x < +l$, ϕ_{III} consists of $\phi_{\mathrm{III}s}$ and $\phi_{\mathrm{III}w}$, in region IV, $l < x < l + b$, ϕ_{IV} consists of $\phi_{\mathrm{IV}s}$and $\phi_{\mathrm{IV}w}$, and in region V, $l + b < x < \infty$, ϕ_{V} consists of $\phi_{\mathrm{V}s}$ and $\phi_{\mathrm{V}w}$. The subscript s denotes the scattering problem and w denotes the radiation (wave making) problem. All of the velocity potentials satisfy the Laplace equation. On the four artificial boundaries, free surface of the water, seabed and the bottom face of the platform, the kinematic boundary conditions must be satisfied and the dynamic boundary

conditions also must be satisfied on the four artificial boundaries and the free surface. Furthermore, on the infinite boundary $-\infty$ in region I and $+\infty$ in region V, the Sommerfeld's radiation condition is satisfied to secure unique solutions

$$\lim_{x\to\pm\infty}\left[\frac{\partial\phi}{\partial x}\pm\frac{1}{c_w}\frac{\partial\phi}{\partial t}\right]=0, \tag{7}$$

where c_w is the celerity of the waves.

3.1. Scattering problem

In the scattering problem, the incident wave is considered as being diffracted by a fixed structure. The corresponding boundary-value problem is shown in Fig. 2(a). Applying the method of the separation of variables, matching the horizontal boundary conditions in each region and applying the Sommerfeld's condition to regions I and V, the velocity potential and the corresponding surface elevation η in each region can be found as given below.

For region I:

$$\phi_{\mathrm{I}s}=\sum_{j=1}^{\infty}\frac{A_{\mathrm{I}sj}g}{\sigma}\frac{\cos[K_j(z+h)]}{\cos(K_jh)}\mathrm{e}^{[K_j(x+l+b)-\mathrm{i}\sigma t]}, \tag{8}$$

$$\eta_{\mathrm{I}s}=-\mathrm{i}\sum_{j=1}^{\infty}A_{\mathrm{I}sj}\mathrm{e}^{[K_j(x+l+b)-\mathrm{i}\sigma t]}. \tag{9}$$

For region V:

$$\phi_{\mathrm{V}s}=\sum_{j=1}^{\infty}\frac{A_{\mathrm{V}j}g}{\sigma}\frac{\cos[K_j(z+h)]}{\cos(K_jh)}\mathrm{e}^{-[K_j(x-l-b)+\mathrm{i}\sigma t]}, \tag{10}$$

$$\eta_{\mathrm{V}s}=-\mathrm{i}\sum_{j=1}^{\infty}A_{\mathrm{V}sj}\mathrm{e}^{-[K_j(x-l-b)+\mathrm{i}\sigma t]}, \tag{11}$$

where the eigenvalues K_j can be solved from the dispersion equation

$$\sigma^2=gK_j\tan(K_jh), \tag{12}$$

where

$$K_1=-\mathrm{i}k,\quad j=1,$$

$$(2j-3)\frac{\pi}{2}<K_jh<(j-1)\pi,\quad j\geqslant 2. \tag{13}$$

For region II:

$$\phi_{\mathrm{II}s}=\frac{ig}{\sigma}\left[\left(A_{\mathrm{II}sP1}\frac{x}{l+b}+A_{\mathrm{II}sN1}\right)\cos K_{\mathrm{II}1}(z+h)\right.$$
$$\left.+\sum_{j=2}^{\infty}(-1)^{j-1}(A_{\mathrm{II}sPj}\mathrm{e}^{-K_{\mathrm{II}j}(x+l+b)}+A_{\mathrm{II}sNj}\mathrm{e}^{K_{\mathrm{II}j}(x-l)})\cos K_{\mathrm{II}j}(z+h)\right]\mathrm{e}^{-\mathrm{i}\sigma t}. \tag{14}$$

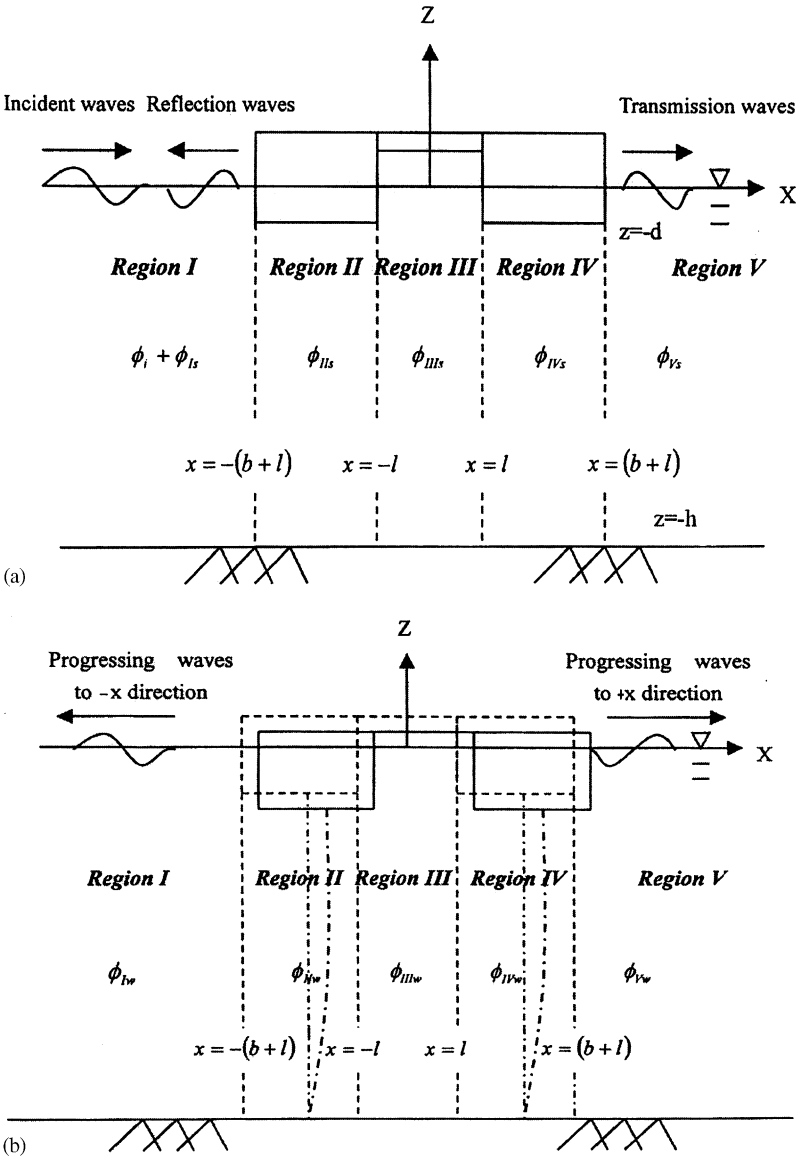

Fig. 2. (a) Illustration of the scattering boundary-value problem. (b) Illustration of the radiation boundary-value problem.

For region IV:

$$\phi_{\mathrm{IV}s} = \frac{\mathrm{i}g}{\sigma}\left[\left(A_{\mathrm{IV}sP1}\frac{x}{l+b} + A_{\mathrm{IV}sN1}\right)\cos K_{\mathrm{II}1}(z+h)\right) + \sum_{j=2}^{\infty}(-1)^{j-1}(A_{\mathrm{IV}sPj}\mathrm{e}^{-K_{\mathrm{II}j}(x+l)} + A_{\mathrm{IV}sNj}\mathrm{e}^{K_{\mathrm{II}j}(x-l-b)})\cos K_{\mathrm{II}j}(z+h)\right]\mathrm{e}^{-\mathrm{i}\sigma t}, \quad (15)$$

where eigenvalue $K_{\mathrm{II}j}$ can also be obtained from the dispersion equation

$$K_{\mathrm{II}j} = \frac{(j-1)\pi}{h-d}, \quad j \geqslant 1, \tag{16}$$

In region III, due to the constraint of its two vertical boundaries, Sommerfeld's radiation conditions are not required to be satisfied. The velocity potential $\phi_{\mathrm{III}s}$ and the free surface elevation $\eta_{\mathrm{III}s}$ are given by

$$\phi_{\mathrm{III}s} = \sum_{j=1}^{\infty} \frac{g}{\sigma}\left[A_{\mathrm{III}sPj}\mathrm{e}^{-K_j(x+l)} + A_{\mathrm{III}sNj}\mathrm{e}^{K_j(x-l)}\right]\frac{\cos K_j(z+h)}{\cos K_j h}\mathrm{e}^{-\mathrm{i}\sigma t} \tag{17}$$

and

$$\eta_{\mathrm{III}s} = -\mathrm{i}\sum_{j=1}^{\infty}\left[A_{\mathrm{III}sPj}\mathrm{e}^{-K_j(x+l)} + A_{\mathrm{III}sNj}\mathrm{e}^{K_j(x-l)}\right]\mathrm{e}^{-\mathrm{i}\sigma t}, \tag{18}$$

where the eigenvalues K_j are similar to those obtained in regions I and V.

In Eqs. (8), (10), (14), (15) and (17), there are totally $8N$ unknowns, where N is the number of terms used in the series, $A_{\mathrm{I}sj}$, $A_{\mathrm{II}sPj}$, $A_{\mathrm{II}sNj}$, $A_{\mathrm{III}sPj}$, $A_{\mathrm{III}sNj}$, $A_{\mathrm{IV}sPj}$, $A_{\mathrm{IV}sNj}$ and $A_{\mathrm{V}sj}$. By applying the kinematic and dynamic boundary conditions on four artificial boundaries for regions II and IV, where $x = -l-b$, $-l$, $+l$ and $l+b$, and taking the advantage of orthogonality of functions, the aforementioned $8N$ unknowns can be solved by $8N$ set of equations simultaneously. Both the kinematic and dynamic boundary conditions are illustrated in Fig. 3 and also written as follows for $\alpha \geqslant 1$:

Kinematic boundary condition (KBC) on $x = -l-b$ between regions I and II:

$$\frac{\partial(\phi_i + \phi_{\mathrm{I}s})}{\partial x} = 0, \quad 0 < z < -d \tag{19}$$

and

$$\frac{\partial(\phi_i + \phi_{\mathrm{I}s})}{\partial x} = \frac{\partial \phi_{\mathrm{II}s}}{\partial x}, \quad -h < z < -d. \tag{20}$$

Dynamic boundary condition (DBC) on $x = -l-b$ between regions I and II:

$$\frac{\partial(\phi_i + \phi_{\mathrm{I}s})}{\partial t} = \frac{\partial \phi_{\mathrm{II}s}}{\partial t}, \quad -h < z < -d. \tag{21}$$

KBC on $x = -l$ between regions II and III:

$$\frac{\partial \phi_{\mathrm{III}s}}{\partial x} = 0, \quad 0 < z < -d. \tag{22}$$

and

$$\frac{\partial \phi_{\mathrm{II}s}}{\partial x} = \frac{\partial \phi_{\mathrm{III}s}}{\partial x}, \quad -h < z < -d. \tag{23}$$

DBC on $x = -l$ between regions II and III:

$$\frac{\partial \phi_{\mathrm{II}s}}{\partial t} = \frac{\partial \phi_{\mathrm{III}s}}{\partial t}, \quad -h < z < -d. \tag{24}$$

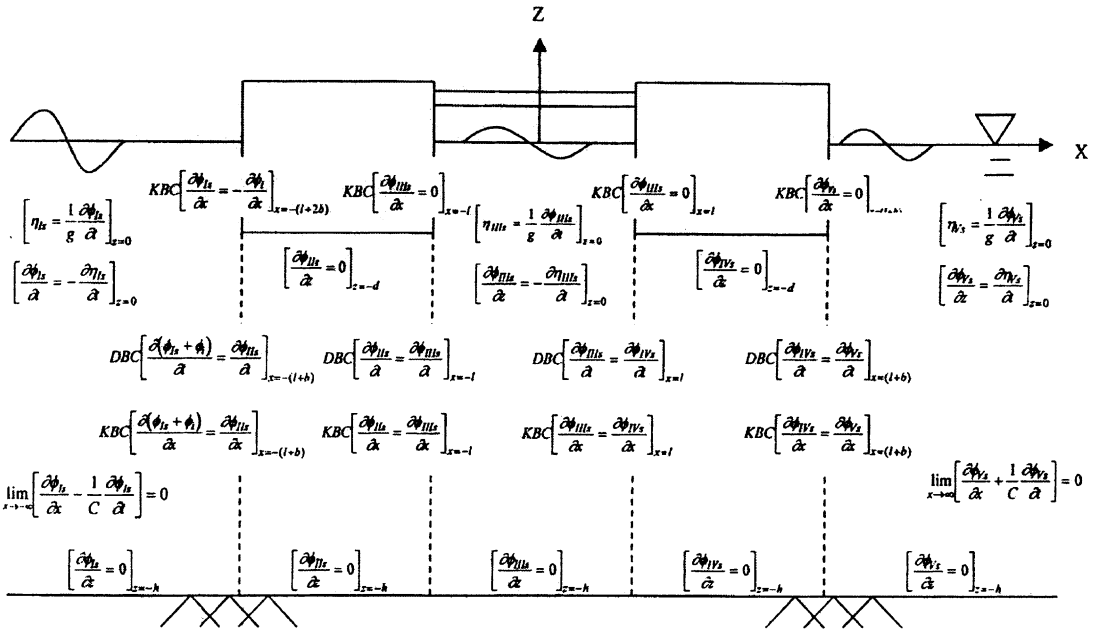

Fig. 3. The kinematic and dynamic boundary conditions on the scattering boundary-value problem.

KBC on $x = l$ between regions III and IV:

$$\frac{\partial \phi_{\mathrm{III}s}}{\partial x} = 0, \quad 0 < z < -d. \tag{25}$$

and

$$\frac{\partial \phi_{\mathrm{III}s}}{\partial x} = \frac{\partial \phi_{\mathrm{IV}s}}{\partial x}, \quad -h < z < -d. \tag{26}$$

DBC on $x = l$ between regions III and IV:

$$\frac{\partial \phi_{\mathrm{III}s}}{\partial t} = \frac{\partial \phi_{\mathrm{IV}s}}{\partial t}, \quad -h < z < -d. \tag{27}$$

KBC on $x = l + b$ between regions IV and V:

$$\frac{\partial \phi_{\mathrm{IV}s}}{\partial x} = 0, \quad 0 < z < -d \tag{28}$$

and

$$\frac{\partial \phi_{\mathrm{IV}s}}{\partial x} = \frac{\partial \phi_{\mathrm{V}s}}{\partial x}, \quad -h < z < -d. \tag{29}$$

DBC on $x = l + b$ between regions IV and V:

$$\frac{\partial \phi_{\mathrm{IV}s}}{\partial t} = \frac{\partial \phi_{\mathrm{V}s}}{\partial t}, \quad -h < z < -d. \tag{30}$$

By employing the orthogonality of the velocity potential functions the boundary conditions can be further derived as eight equations on the four boundaries in terms of the $8N$ unknowns to be solved for velocity potential as shown by Eqs. (A.1)–(A.8) in Appendix A.

3.2. Radiation problem

In the radiation problem, the structure is considered to be forced in motion by the wave force induced by incident waves and scattered waves and then the structure motion results in waves propagating in the x direction similar to a wave maker. The corresponding boundary-value problem is illustrated in Fig. 2(b). The displacement of the surge motion of the platform is given by

$$\xi = S\mathrm{e}^{-\mathrm{i}\sigma t} \tag{31}$$

where S is the unknown amplitude of the surge motion. By means of the method similar to the scattering problem, in this radiation problem, the velocity potential and the corresponding elevation of free surface are written as follows:

For region I:

$$\phi_{\mathrm{I}w} = \sum_{j=1}^{\infty} \frac{A_{\mathrm{I}wj} g}{\sigma} \frac{\cos[K_j(z+h)]}{\cos(K_j h)} \mathrm{e}^{[K_j(x+l+b)-\mathrm{i}\sigma t]}, \tag{32}$$

$$\eta_{\mathrm{I}w} = -\mathrm{i} \sum_{j=1}^{\infty} A_{\mathrm{I}wj} e^{[K_j(x+l+b)-\mathrm{i}\sigma t]}. \tag{33}$$

For region II:

$$\phi_{\mathrm{II}w} = \frac{\mathrm{i}g}{\sigma}\left[\left(A_{\mathrm{II}wP1}\frac{x}{l+b} + A_{\mathrm{II}wN1}\right)\cos K_{\mathrm{II}1}(z+h) + \sum_{j=2}^{\infty}(-1)^{j-1}(A_{\mathrm{II}wPj}\mathrm{e}^{-K_{\mathrm{II}j}(x+l+b)} + A_{\mathrm{II}wNj}\mathrm{e}^{K_{\mathrm{II}j}(x-l)})\cos K_{\mathrm{II}j}(z+h)\right]\mathrm{e}^{-\mathrm{i}\sigma t}. \tag{34}$$

For region III:

$$\phi_{\mathrm{III}w} = \sum_{j=1}^{\infty} \frac{g}{\sigma}\left[A_{\mathrm{III}wPj}\mathrm{e}^{-K_j(x+l)} + A_{\mathrm{III}wNj}\mathrm{e}^{K_j(x-l)}\right]\frac{\cos[K_j(z+h)]}{\cos(K_j h)}\mathrm{e}^{-\mathrm{i}\sigma t}, \tag{35}$$

$$\eta_{\mathrm{III}w} = -\mathrm{i}\sum_{j=1}^{\infty}\left[A_{\mathrm{III}wPj}\mathrm{e}^{-K_j(x+l)} + A_{\mathrm{III}wNj}\mathrm{e}^{K_j(x-l)}\right]\mathrm{e}^{-\mathrm{i}\sigma t}. \tag{36}$$

For region IV:

$$\phi_{\mathrm{IV}w} = \frac{\mathrm{i}g}{\sigma}\left[\left(A_{\mathrm{IV}wP1}\frac{x}{l+b} + A_{\mathrm{IV}wN1}\right)\cos K_{\mathrm{II}1}(z+h) + \sum_{j=2}^{\infty}(-1)^{j-1}(A_{\mathrm{IV}wPj}e^{-K_{\mathrm{II}j}(x+l)} + A_{\mathrm{IV}wNj}\mathrm{e}^{K_{\mathrm{II}j}(x-l-b)})\cos K_{\mathrm{II}j}(z+h)\right]\mathrm{e}^{-\mathrm{i}\sigma t}. \tag{37}$$

For region V:

$$\phi_{\mathrm{V}w} = \sum_{j=1}^{\infty} \frac{A_{\mathrm{V}wj} g}{\sigma} \frac{\cos[K_j(z+h)]}{\cos(K_j h)} \mathrm{e}^{-[K_j(x-l-b)+\mathrm{i}\sigma t]}, \tag{38}$$

$$\eta_{\mathrm{V}w} = \sum_{j=1}^{\infty} A_{\mathrm{V}wj} \mathrm{e}^{-[K_j(x-l-b)+\mathrm{i}\sigma t]}, \tag{39}$$

where the eigenvalues K_j remain the same as those in the scattering problem. In Eqs. (32), (34), (35), (37) and (38) there are totally $8N$ unknowns, $A_{\mathrm{I}wj}$, $A_{\mathrm{II}wPj}$, $A_{\mathrm{II}wNj}$, $A_{\mathrm{III}wPj}$, $A_{\mathrm{III}wNj}$, $A_{\mathrm{IV}wPj}$, $A_{\mathrm{IV}wNj}$ and $A_{\mathrm{V}wj}$. Similarly, by applying the kinematic and dynamic boundary conditions on four artificial boundaries of regions II and IV, and taking the advantage of orthogonality of the functions, the $8N$ unknowns can be solved by $8N$ set of equations simultaneously. Boundary conditions associated with the radiation problem are illustrated in Fig. 4 and equations derived from the boundary conditions are written as follows for $\alpha \geqslant 1$:

KBC on $x = -l - b$ between regions I and II:

$$-\frac{\partial \phi_{\mathrm{I}w}}{\partial x} = \frac{\mathrm{d}\xi}{\mathrm{d}t}, \quad 0 < z < -d \tag{40}$$

and

$$\frac{\partial \phi_{\mathrm{I}w}}{\partial x} = \frac{\partial \phi_{\mathrm{II}w}}{\partial x}, \quad -h < z < -d. \tag{41}$$

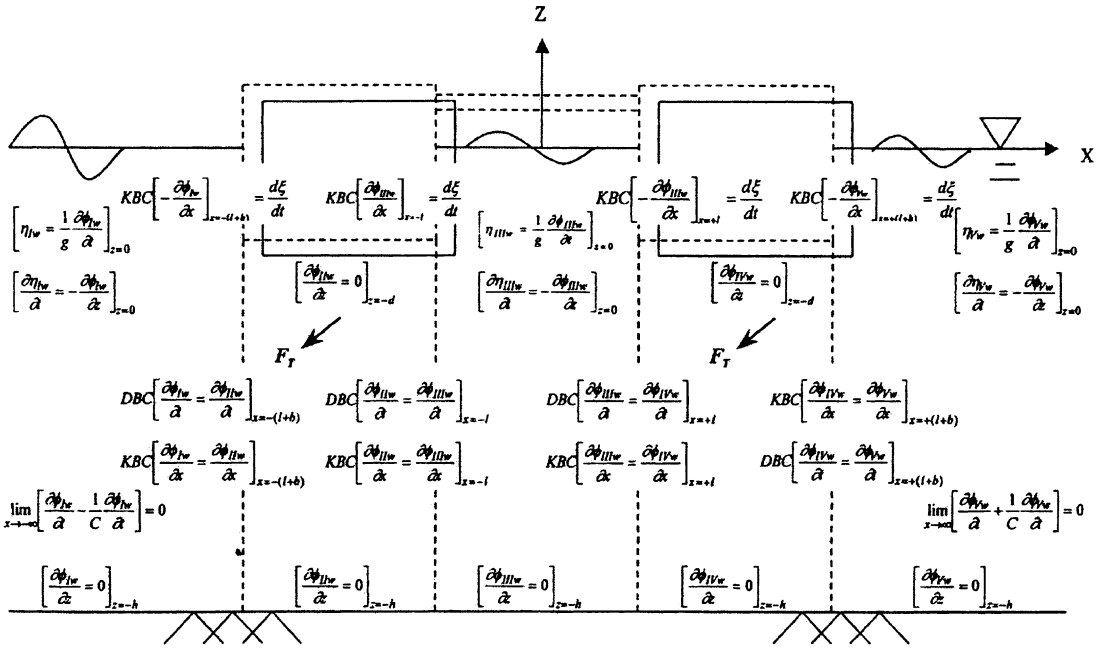

Fig. 4. The kinematic and dynamic boundary conditions on the radiation boundary-value problem.

DBC on $x = -l - b$ between regions I and II:

$$\frac{\partial \phi_{\mathrm{I}w}}{\partial t} = \frac{\partial \phi_{\mathrm{II}w}}{\partial t}, \quad -h < z < -d. \tag{42}$$

KBC on $x = -l$ between regions II and III:

$$\frac{\partial \phi_{\mathrm{III}w}}{\partial x} = \frac{\mathrm{d}\xi}{\mathrm{d}t}, \quad 0 < z < -d \tag{43}$$

and

$$\frac{\partial \phi_{\mathrm{II}w}}{\partial x} = \frac{\partial \phi_{\mathrm{III}w}}{\partial x}, \quad -h < z < -d. \tag{44}$$

DBC on $x = -l$ between regions II and III:

$$\frac{\partial \phi_{\mathrm{II}w}}{\partial t} = \frac{\partial \phi_{\mathrm{III}w}}{\partial t}, \quad -h < z < -d. \tag{45}$$

KBC on $x = l$ between regions III and IV:

$$-\frac{\partial \phi_{\mathrm{III}w}}{\partial x} = \frac{\mathrm{d}\xi}{\mathrm{d}t}, \quad 0 < z < -d \tag{46}$$

and

$$\frac{\partial \phi_{\mathrm{III}w}}{\partial x} = \frac{\partial \phi_{\mathrm{IV}w}}{\partial x}, \quad -h < z < -d. \tag{47}$$

DBC on $x = l$ between regions III and IV:

$$\frac{\partial \phi_{\mathrm{III}w}}{\partial t} = \frac{\partial \phi_{\mathrm{IV}w}}{\partial t}, \quad -h < z < -d. \tag{48}$$

KBC on $x = l + b$ between regions IV and V:

$$-\frac{\partial \phi_{\mathrm{V}w}}{\partial x} = \frac{\mathrm{d}\xi}{\mathrm{d}t}, \quad 0 < z < -d \tag{49}$$

and

$$\frac{\partial \phi_{\mathrm{IV}w}}{\partial x} = \frac{\partial \phi_{\mathrm{V}w}}{\partial x}, \quad -h < z < -d. \tag{50}$$

DBC on $x = l + b$ between regions IV and V:

$$\frac{\partial \phi_{\mathrm{IV}w}}{\partial t} = \frac{\partial \phi_{\mathrm{V}w}}{\partial t}, \quad -h < z < -d. \tag{51}$$

By employing the orthogonality of the velocity potential functions the boundary conditions can be further derived into equations as shown by Eqs. (A.9)–(A.16) of Appendix A, in terms of the form of velocity potential that includes $8N$ unknowns to be solved.

As was observed in these $8N$ series of equations, in addition to the aforementioned $8N$ set of unknowns, due to the displacement of the platform, there is one more unknown S, the amplitude of the surge motion, to be solved. Therefore, to solve for the amplitude S one additional set of equation, the equation of the surge motion of the platform, is required.

3.3. Motion of the platform

The equation of motion of the platform derived from Newton's second law, after neglecting the higher order non-linear term ξ^2 resulted from the dynamic tension of the tether motion, can be written as

$$M\frac{\mathrm{d}^2\xi}{\mathrm{d}t^2} + K^*\xi = F_w + F_{D1} + F_{D2}, \tag{52}$$

where M is the mass of the platform system, F_w is the horizontal wave force exerting on the platform and K^* represents the equivalent stiffness of the platform system induced by the pre-tensioned tethers [6]. The equivalent stiffness of the platform system is given by

$$K^* = \frac{2\rho_w g b}{\ell}(d - d_0)\left(\frac{\mu}{\mu + 1}\right), \tag{53}$$

where $\ell = h - d$, $d_0 = M/(2\rho_w b)$, d_0 and d are drafts of the structure before and after applying the pre-tension force. μ is the proportional stiffness parameter defined as the ratio between the tether stiffness and the buoyancy force of the platform submerged in the water of unit depth.

For the wave force, by applying the linearized Bernoulli equation, the wave force F_w can be obtained through the integration of the total hydrodynamic pressure over the vertical surfaces of the structure on boundaries$x = -(l + b)$, $-l$, $+l$ and $(l + b)$, and given by

$$F_w = \rho_w \int_{-d}^{0} \left(\frac{\partial \phi_{\mathrm{I}}}{\partial t}|_{x=-l-b} + \frac{\partial \phi_{\mathrm{III}}}{\partial t}|_{x=+l} - \frac{\partial \phi_{\mathrm{III}}}{\partial t}|_{x=-l} - \frac{\partial \phi_{\mathrm{V}}}{\partial t}|_{x=+l+b} \right) \mathrm{d}z. \tag{54}$$

$F_{D1/D2}$ are forces exerting on two tether legs due to the drag and inertial effect induced by waves, which may be presented by employing the modified Morison's equation [10] since the diameter of the tether D is small compared to the wavelength as

$$F_{D1/D2} = \int_{-h}^{-d} \left[\tfrac{1}{2}\rho_w D C_D(u - \dot{\chi})(u - \dot{\chi}) + \tfrac{1}{4}\pi\rho_w D^2 C_m(\dot{u} - \ddot{\chi}) + \tfrac{1}{4}\pi\rho_w D^2 \ddot{\chi}\right] \mathrm{d}z, \tag{55}$$

where χ is the horizontal deflection of the tether, while C_D and C_m are the coefficients corresponding to the drag and inertial effect respectively. By applying Lorent's hypothesis of equivalent work [11] and assuming that the linear drag consumes the same energy within one wave period as that of non-linear drag, a linear drag coefficient R_D^* can be defined as

$$Rd^* = \frac{\int_{-h}^{-d}\int_0^T \{[0.5\rho_w D C_d|u - \dot{\chi}|(u - \dot{\chi})](u - \dot{\chi})\}\,\mathrm{d}t\,\mathrm{d}z}{\int_{-h}^{-d}\int_0^T [\rho_w D\sigma(u - \dot{\chi})(u - \dot{\chi})]\,\mathrm{d}t\,\mathrm{d}z}. \tag{56}$$

After substitution for the non-linear drag terms, the forces on the tethers are given as

$$F_{D1/D2} = \int_{-h}^{-d} \left[\rho_w D\sigma R_D^*(u - \dot{\chi}) + \tfrac{1}{4}\pi\rho_w D^2 C_m(\dot{u} - \ddot{\chi}) + \tfrac{1}{4}\pi\rho_w D^2 \ddot{\chi}\right] \mathrm{d}z. \tag{57}$$

For the application of force, $F_{D1/D2}$, the velocity and acceleration for both the fluid and the tether must be obtained first. However, due to the interactions among the wave, platform structure and

tethers, the force, $F_{D1/D2}$, will be applied in terms of the parameters that are to be solved simultaneously together with the structural motion and the flow field. Furthermore, the tether motion χ must also be realized through solving the equation of motion for the tethers subjected to wave forces.

3.4. Motion of the pre-tension tethers

The equation of motion for each pre-tension tether subjected to the wave-induced forces and surge motion of the top platform can be written as

$$\rho\frac{\partial^2\chi}{\partial t^2}+C\frac{\partial\chi}{\partial t}-T^*\frac{\partial^2\chi}{\partial z^2}=f_D, \tag{58}$$

where ρ is the mass of unit length of tether, T^* is the pre-tension force in the platform system and C is the damping coefficient of unit length of the tether. Similarly, the wave force exerted on the unit length of the tether is obtained through Morison's equation for small body, while the relative motion between the fluid and the tether is accounted for. As is presented in Eq. (55) and then modified in Eq. (57) without the integration along the water depth, the wave force, f_D, on unit length of the tether is shown as

$$f_D=\rho_w D\sigma Rd^{**}(u-\dot\chi)+0.25\pi\rho_w D^2C_m(\dot u-\ddot\chi)+0.25\pi\rho_w D^2\ddot\chi, \tag{59}$$

where

$$Rd^{**}=\frac{\int_0^T\{[0.5\rho_w DC_d|u-\dot\chi|(u-\dot\chi)](u-\dot\chi)\}\,\mathrm{d}t}{\int_0^T[\rho_w D\sigma(u-\dot\chi)(u-\dot\chi)]\,\mathrm{d}t}.$$

After substitution of Eq. (59), Eq. (58) can be rewritten in the form as

$$\begin{aligned}&\big[\rho+0.25\pi\rho_w D^2(C_m-1)\big]\frac{\partial^2\chi}{\partial t^2}+\big(C+Rd^{**}\rho_w D\sigma\big)\frac{\partial\chi}{\partial t}-T^*\frac{\partial^2\chi}{\partial z^2}\\&\quad=0.25\pi\rho_w D^2C_m\dot u+Rd^{**}\rho_w D\sigma u.\end{aligned} \tag{60}$$

The velocity of fluid in the equation is obtained from the potential, as was obtained in the large-body problem combined with the scattering and the radiation problem, thus in region II $u=-\partial\phi_{\mathrm{II}}/\partial x$, in region VI $u=-\partial\phi_{\mathrm{VI}}/\partial x$ and $\dot u=\partial u/\partial t$. Substituting u and $\dot u$ in terms of potential derivatives into Eq. (60) we have the equation of motion for the tether in region II as

$$\begin{aligned}&\big[\rho+0.25\pi\rho_w D^2(C_m-1)\big]\frac{\partial^2\chi}{\partial t^2}+\big(C+Rd^{**}\rho_w D\sigma\big)\frac{\partial\chi}{\partial t}-T^*\frac{\partial^2\chi}{\partial z^2}\\&=-\big(0.25\pi\rho_w D^2C_mg+\mathrm{i}Rd^{**}g\rho_w D\big)\left\{\frac{A_{\mathrm{II}s/wP1}}{l+b}\cos K_{\mathrm{II}1}(z+h)\right.\\&\quad\left.+\sum_{n=2}^{\infty}(-1)^{n-1}\big[-K_{\mathrm{II}n}A_{\mathrm{II}s/wPn}\mathrm{e}^{-K_{\mathrm{II}n}(x_1+l+b)}+K_{\mathrm{II}n}A_{\mathrm{II}s/wNn}\mathrm{e}^{(x_1-l)K_{\mathrm{II}n}}\big]\cos K_{\mathrm{II}n}(z+h)\right\}\mathrm{e}^{-\mathrm{i}\sigma t}\end{aligned} \tag{61}$$

and the equation of motion for tether in region VI as

$$[\rho + 0.25\pi\rho_w D^2(C_m - 1)]\frac{\partial^2\chi}{\partial t^2} + \left(C + R^{**}_{d2}\rho_w D\sigma\right)\frac{\partial\chi}{\partial t} - T^*\frac{\partial^2\chi}{\partial z^2}$$
$$= -[0.25\pi\rho_w D^2 C_m g + \mathrm{i}R^{**}_{d1}\cdot g\rho_w D]\left\{\frac{A_{\mathrm{IV}s/wP1}}{l+b}\cos K_{\mathrm{II}1}(z+h)\right.$$
$$\left. + \sum_{n=2}^{\infty}(-1)^{n-1}\left[-K_{\mathrm{IV}n}A_{\mathrm{IV}s/wPn}\mathrm{e}^{-K_{\mathrm{II}n}(x_2+l)} + K_{\mathrm{IV}n}A_{\mathrm{IV}s/wNn}\mathrm{e}^{(x_2-l-b)K_{II_n}}\right]\cos K_{\mathrm{IV}n}(z+h)\right\}\mathrm{e}^{-\mathrm{i}\sigma t}. \quad (62)$$

The motion of the tether at the joint connected to the platform structure will be same as the motion of the platform, that was assumed to be harmonic with amplitude S and frequency σ, as $\chi(-d,t) = S\mathrm{e}^{-\mathrm{i}\sigma t}$, and on the sea bed the motion is restrained thus, $\chi(-h,t) = 0$. Assuming that the motion of the tether is in the same harmonic form as the platform $\chi(z,t) = Z(z)\mathrm{e}^{-\mathrm{i}\sigma t}$, and substituting back in the equation of motion, a reduced equation of motion for the tether can be obtained such as the tether in region II given by

$$T^*\frac{\mathrm{d}^2Z}{\mathrm{d}z^2} + \{[\rho + 0.25\pi\rho_w D^2(C_m - 1)]\sigma^2 + (C + Rd^{**}\rho_w D\sigma)(\mathrm{i}\sigma)^2\}Z(z)$$
$$= (0.25\pi\rho_w D^2 C_m g + \mathrm{i}Rd^{**}g\rho_w D)\left\{\frac{A_{\mathrm{II}s/wP1}}{b}\cos K_{\mathrm{II}1}(z+h)\right.$$
$$\left. + \sum_{n=2}^{\infty}(-1)^{n-1}(-K_{\mathrm{II}n}A_{\mathrm{II}s/wPn} + K_{\mathrm{II}s/wNn}\mathrm{e}^{-2bK_{\mathrm{II}n}})\cos K_{\mathrm{II}n}(z+h)\right\} \quad (63)$$

along with reduced boundary conditions as

$$\begin{cases} Z(-d) = S, \\ Z(-h) = 0. \end{cases}$$

After solving the equation the relationship between the tether motion and the flow field is established such as the tether in region II is given by

$$\chi(z,t) = \left[C_1\mathrm{e}^{az} + C_2\mathrm{e}^{-az} + \sum_{n=1}^{\infty}a_n\cos K_{\mathrm{II}n}(z+h)\right]\mathrm{e}^{-\mathrm{i}\sigma t}, \quad (64)$$

where the coefficients a, C_1, C_2 and a_n are related to the tether behavior in region II. A similar equation for the tether in region VI can also be obtained with coefficients a^*, C_1^*, C_2^* and a_n^*. These parameters are all defined and listed in Appendix B.

3.5. Complete equation of motion for platform structure

By substituting the velocity potentials of regions I, III and V into Eq. (54) and then substituting Eq. (54) and (57) back into Eq. (52), the complete equation of motion for the platform that takes

account of the multi-interaction effects can be written as

$$
\begin{aligned}
&M\frac{\mathrm{d}^2\xi}{\mathrm{d}t^2}-\rho\int_{-d}^{0}\left(\frac{\partial\phi_{\mathrm{I}w}}{\partial t}|_{x=-l-b}+\frac{\partial\phi_{\mathrm{III}w}}{\partial t}|_{x=+l}-\frac{\partial\phi_{\mathrm{III}w}}{\partial t}\right|_{x=-l}-\frac{\partial\phi_{\mathrm{V}w}}{\partial t}|_{x=l+b}\Bigg)\,\mathrm{d}z+K^{*}\xi\\
&\quad=\rho\int_{d}^{0}\left(\frac{\partial(\phi_i+\phi_{\mathrm{I}s}}{\partial t}|_{x=-l-b}+\frac{\partial\phi_{\mathrm{III}s}}{\partial t}|_{x=l}-\frac{\partial\phi_{\mathrm{III}s}}{\partial t}\right|_{x=-l}-\frac{\partial\phi_{\mathrm{V}s}}{\partial t}|_{x=l+b}\Bigg)\,\mathrm{d}z\\
&\qquad+\rho_w D\sigma\int_{-h}^{-d}R_{d1}\left(-\frac{\partial\phi_{\mathrm{II}s}}{\partial x}|_{x=x_1-l-b}\right)\mathrm{d}z+\rho_w D\sigma^2\left(0.25\pi D(C_m-1)+\mathrm{i}R_{d1}^{*}\right)\lambda_1|_{x=x_1-l-b}\\
&\qquad+\rho_w D\sigma\int_{-h}^{d}R_{d1}\left(-\frac{\partial\phi_{\mathrm{II}w}}{\partial x}|_{x=x_1-l-b}\right)\mathrm{d}z\\
&\qquad+\rho_w D\sigma\int_{-h}^{-d}R_{d2}\left(-\frac{\partial\phi_{\mathrm{IV}s}}{\partial x}|_{x=x_2+l+b}\right)\mathrm{d}z+\rho_w D\sigma^2\left(0.25\pi D(C_m-1)+\mathrm{i}R_{d2}^{*}\right)\lambda_2|_{x=x_2+l+b}\\
&\qquad+\rho_w D\sigma\int_{-h}^{d}R_{d2}\left(-\frac{\partial\phi_{\mathrm{IV}w}}{\partial x}|_{x=x_2+l+b}\right)\mathrm{d}z,
\end{aligned}
\tag{65}
$$

where $R_{d1/d2}=R_{d1/d2}^{*}-0.25\mathrm{i}D\pi C_m$, parameters λ_1 and λ_2 are given in Appendix C. In the equation, the potential terms with subscript w represent the effect induced from radiated waves while terms with subscript s denote the scattered wave effect. After carrying out the integration and rearrangement, the equation can further be expressed in terms of coefficients of potential and platform amplitudes as

$$
\begin{aligned}
&-\rho_W\left[\sum_{n=1}^{\infty}\frac{(-\mathrm{i}g)}{\cos K_n h}\langle Z_n^0\rangle\right]A_{\mathrm{I}wn}-[\varsigma_1]A_{\mathrm{II}wP1}\\
&-\left[\sum_{n=2}^{\infty}(G_n\mathrm{e}^{-K_{\mathrm{II}n}(x_1+l+b)}-\beta\Gamma_n\mathrm{e}^{-K_{\mathrm{II}n}(x_1+l+b)})\right]A_{\mathrm{II}wPn}\\
&+\left[\sum_{n=2}^{\infty}(G_n\mathrm{e}^{K_{\mathrm{II}n}(x_1-l)}-\beta\Gamma_n\mathrm{e}^{K_{\mathrm{II}n}(x_1-l)})\right]A_{\mathrm{II}wNn}\\
&-\rho_W\left[\sum_{n=1}^{\infty}\frac{(-\mathrm{i}g)}{\cos K_n h}\langle Z_n^0\rangle(\mathrm{e}^{-2lK_n}-1)\right]A_{\mathrm{III}wPn}\\
&-\rho_W\left[\sum_{n=1}^{\infty}\frac{(-\mathrm{i}g)}{\cos K_n h}\langle Z_n^0\rangle(1-\mathrm{e}^{-2lK_n})\right]A_{\mathrm{III}wNn}-\left[\varsigma_1^{*}\right]A_{\mathrm{IV}wP1}\\
&-\left[\sum_{n=2}^{\infty}(G_n^{*}\mathrm{e}^{-K_{\mathrm{II}n}(x_2+l)}-\beta^{*}\Gamma_n^{*}\mathrm{e}^{-K_{\mathrm{II}n}(x_2+l)})\right]A_{\mathrm{IV}wPn}\\
&+\left[\sum_{n=2}^{\infty}(G_n^{*}\mathrm{e}^{K_{\mathrm{II}n}(x_2-l-b)}-\beta^{*}\Gamma_n^{*}\mathrm{e}^{K_{\mathrm{II}n}(x_2-l-b)})\right]A_{\mathrm{IV}wNn}
\end{aligned}
$$

$$
\begin{aligned}
&+\rho_W\left[\sum_{n=1}^{\infty}\frac{(-\mathrm{i}g)}{\cos K_n h}\langle Z_n^0\rangle\right]A_{\mathrm{V}wn}+\left[K-\sigma^2M-(\beta Q+\beta^* Q^*)\right]S\\
&=\rho_w\left[\frac{-\mathrm{i}A_i g}{\cos K_1 h}\mathrm{e}^{K_1 b}\langle Z_1^0\rangle\right]\\
&\quad+\rho_W\left[\sum_{n=1}^{\infty}\frac{(-\mathrm{i}g)}{\cos K_n h}\langle Z_n^0\rangle\right]A_{\mathrm{I}sn}+[\varsigma_1]A_{\mathrm{II}sP1}\\
&\quad+\left[\sum_{n=2}^{\infty}(G_n\mathrm{e}^{-K_{\mathrm{II}n}(x_1+l+b)}-\beta\Gamma_n\mathrm{e}^{-K_{\mathrm{II}n}(x_1+l+b)})\right]A_{\mathrm{II}sPn}\\
&\quad-\left[\sum_{n=2}^{\infty}(G_n\mathrm{e}^{K_{\mathrm{II}n}(x_1-l)}-\beta\Gamma_n\mathrm{e}^{K_{\mathrm{II}n}(x_1-l)})\right]A_{\mathrm{II}sNn}\\
&\quad+\rho_W\left[\sum_{n=1}^{\infty}\frac{(-\mathrm{i}g)}{\cos K_n h}\langle Z_n^0\rangle(\mathrm{e}^{-2lK_n}-1)\right]A_{\mathrm{III}sPn}\\
&\quad+\rho_W\left[\sum_{n=1}^{\infty}\frac{(-\mathrm{i}g)}{\cos K_n h}\langle Z_n^0\rangle(1-\mathrm{e}^{-2lK_n})\right]A_{\mathrm{III}sNn}+\left\lfloor\varsigma_1^*\right\rfloor A_{\mathrm{IV}sP1}\\
&\quad+\left[\sum_{n=2}^{\infty}(G_n^*\mathrm{e}^{-K_{\mathrm{II}n}(x_2+l)}-\beta^*\Gamma_n^*\mathrm{e}^{-K_{\mathrm{II}n}(x_2+l)})\right]A_{\mathrm{IV}sPn}\\
&\quad-\left[\sum_{n=2}^{\infty}(G_n^*\mathrm{e}^{K_{\mathrm{II}n}(x_2-l-b)}-\beta^*\Gamma_n^*\mathrm{e}^{K_{\mathrm{II}n}(x_2-l-b)})\right]A_{\mathrm{IV}sNn}\\
&\quad-\rho_W\left[\sum_{n=1}^{\infty}\frac{(-\mathrm{i}g)}{\cos K_n h}\langle Z_n^0\rangle\right]A_{\mathrm{V}sn},
\end{aligned}
\tag{66}
$$

where the parameters $\beta, \beta^*, Q, Q^*, \Gamma_n, \Gamma_n^*, \varsigma_1, \varsigma_1^*, G_n$ and G_n^* are also presented in Appendix C. With Eq. (66) and Eqs. (A.9)–(A.16) derived from Eqs. (40)–(51), the aforementioned $8N+1$ unknowns in the radiation problem can be solved simultaneously. By substituting these solutions back into Eqs. (A.1) to (A.8), which were derived from Eqs. (19) to (30), the dragged surge motion of the twin platform, the velocity potential, the corresponding elevation of the free surface in each region and the velocity of the flow can also be calculated when the multi-interactions among waves, platform and the pretension tethers are all taken into consideration.

4. Numerical results and discussions

To demonstrate the analytical solution, numerical examples are presented in this section. Since the analytical solution is in an infinite series form, the convergence of the solution was also demonstrated and discussed. As was mentioned in the Introduction, the twin-platform system is more close to the practical application even though the analysis is more challenging. Therefore, in the numerical examples a comparison between the single- and the twin-platform system was also

made when the spacing between two platforms of the twin-platform system was reduced thus becoming similar to a single-platform system. The platform responses due to coupled interactions among the waves, platform and the tethers were obtained and compared to the cases without tether–wave interactions.

Influences resulting from the structural factors such as the spacing between two platforms, platform dimensions and the influence of water depth, were discussed in the examples, while the material related parameters remained constant, which were discussed in the single-platform analysis. The influence from the mass and the draft of the platform was also presented and discussed shortly to examine the similarity to the single-platform system. The analysis was focused on the amplitude of the surge motion of the platform and the reflection coefficient of the wave, both corresponding to the dimensionless frequency of incident waves. Furthermore, the resonant phenomenon for the free water surface between two platforms similar to harbor seiching was also observed and discussed.

4.1. The convergence and consistency of the solution

Two tests were performed here for the analytical solutions of this twin-platform system, namely the convergence of the series solution and the consistency of the solution when reduced to a single-platform system. The convergence test for appropriate wave modes in the series solution was performed when related factors such as the incident wave height, wave period, water depth and the geometry of the structure were taken into account. Assuming that the convergent error is set to be 5%, for wave periods ranging from 2 to 20 s, the convergence of the reflection coefficient K_r corresponding to the number of wave modes in the series solution is shown in Fig. 5(a) and (b). The parameters related to the structure and water depth are also shown in the figure. It shows that after 15, mostly less than 10, wave modes, all of the reflection coefficients approach a value within the range of the convergent error.

Next, consistency between the single- and twin-platform solution was examined when the spacing between two platforms vanished, $l=0$. Fig. 6(a) shows the dimensionless amplitude of the surge motion of the twin-platform system corresponding to the dimensionless frequency of the incident wave, $\sigma^2 g/h$, applied to the platform system located in the water 30.0 m deep. As was shown, the responses resulting from twin-platform and single-platform systems almost merged into one. Fig. 6(b) presented the reflection and transmission coefficients of the wave for both the reduced twin- and single-platform systems corresponding to the frequency of the incident wave. Again, both the reflection and the transmission coefficients were matched into the same curve for the two platform systems. Therefore, the solution for the twin-platform system is consistent with that of the single platform and able to solve a single-platform system problem when the multi-interactions among waves, platform and strained tethers are taken into account.

4.2. Influence of twin-platform parameters on the structural motion

4.2.1. The spacing effect on the twin-platform drag surge motion

The tether drag effect corresponding to the influence of spacing between two platforms in the twin-platform system was examined here. In the numerical example the dimension of each platform remained constant while the spacing between them varied. Fig. 7(a) shows the

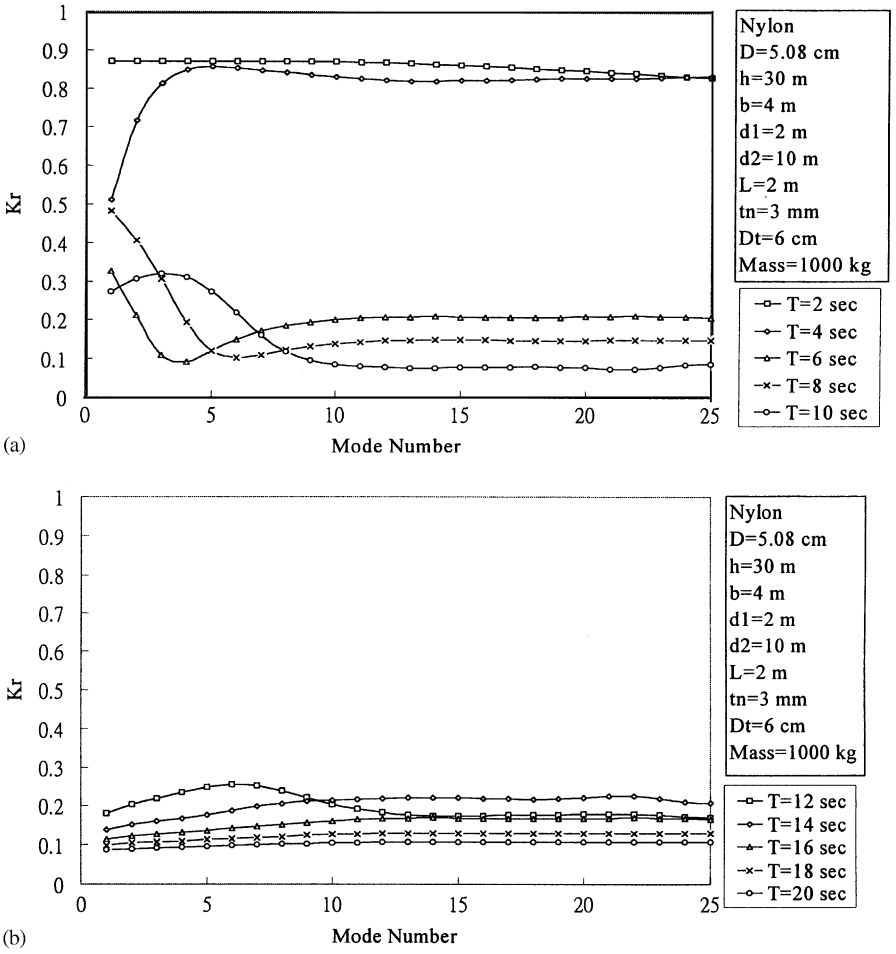

Fig. 5. The convergence of the reflection coefficient corresponding to the number of mode for the series solution. (a) Wave period from 2 to 10 s. (b) Wave period from 12 to 20 s.

dimensionless amplitude of the platform drag surge motion while Fig. 7(b) is the response comparison to the platform without tether–wave interactions. The corresponding dimension and related parameters are also presented in the figure. In Fig. 7(a) both the amplitude of the drag surge motion and the resonant period of the response were increased corresponding to the increase of the spacing between two platforms. However, when the spacing reached 8 m, ratio $b/l = 0.5$, the amplitude seemed to converge to a constant. Compared to the case where the tether–wave interactions are not taken into account, as observed from Fig. 7(b) the trend of the amplitude variation corresponding to the frequency of the incident waves is quite similar to each other except that the amplitude was greatly reduced from the tether–wave interaction effect.

4.2.2. The dimension effect on the twin-platform drag surge motion

The dimension of each single platform for the twin-platform system was varied for the examination of the influence on the drag surge motion of the platform system. Fig. 8(a) is the

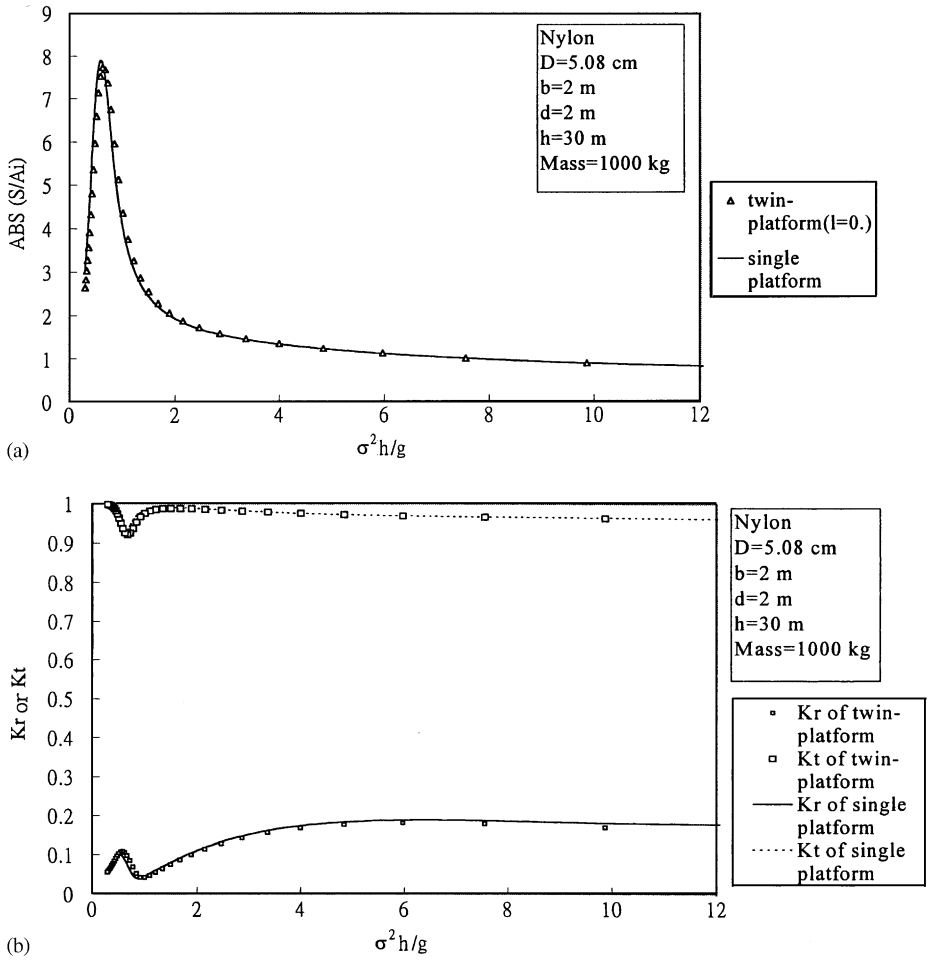

Fig. 6. The consistency for the solution between the single platform and twin-platform system. Comparison of the dimensionless response amplitude of the platform. Comparison of the reflection and transmission coefficients.

reflection coefficient of the platform system corresponding to the dimensionless frequency of the incident wave. Influenced by the tether–wave interactions the maximum value of the coefficients is not a unit value anymore such as the case without tether–wave interactions but varied such that corresponding to the increase of the platform dimension the reflection coefficients are increased. Fig. 8(b) shows comparisons of dimensionless amplitude of platform motions between platforms with and without considering the tether–wave interactions. For the case without considering the tether effect, corresponding to the increase of the dimension of each platform, both the amplitude and the resonant period of the platform surge motion decreased significantly. However, for the case where the tether effect is considered, corresponding to the increase of the platform dimension, the amplitude only reduced slightly. The difference in the amplitude between two cases is larger when the platform dimension is smaller. It is because the correspondingly smaller system stiffness would allow a larger vibration on the tether, which due to the tether–wave interaction would damp more energy and then reduce the platform motion more significantly.

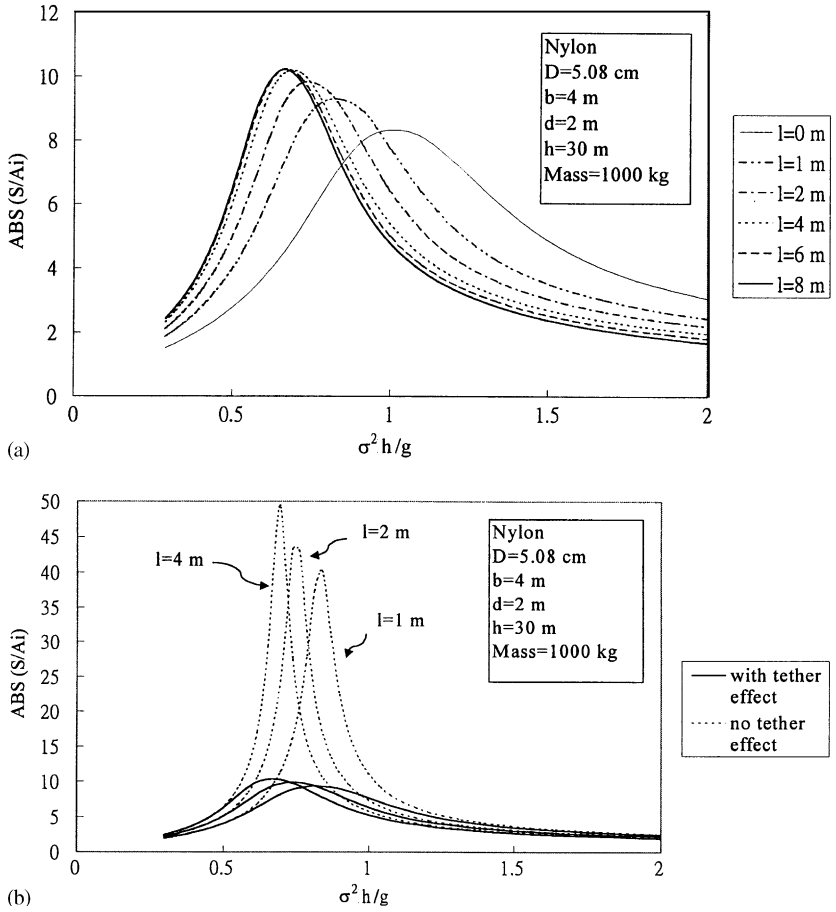

Fig. 7. The dragged surge motion response for the twin-platform system with respect to the variation of spacing between two platforms *l*. (a) The dimensionless amplitude of the dragged surge motion corresponding to the wave frequency. (b) The motion comparison between the platforms with and without tether–wave interactions.

4.2.3. The draft effect on the twin-platform drag surge motion

An examination on the influence of the submerged depth of the structure *d*, when the tether–wave interaction effect was accounted for, was carried out here. The platform draft not only affects the eigenvalue of the solution but also the equivalent stiffness K^*. A twin platform each 4.0 m wide was analyzed while the after-tension draft of the platform was varied from 1.0 to 7.0 m. Similar to the previous analysis, Fig. 9(a) and (b) shows the reflection coefficients for the wave and the comparison of the dimensionless amplitudes for platform motions with and without considering the tether–wave interactions corresponding to the dimensionless frequency of the incident waves. The related parameters of the system are also shown in the figure. As shown in Fig. 9(a), influenced by the tether-wave interactions corresponding to the increase of the draft, the reflection coefficient becomes larger while the resonant frequency becomes smaller.

It is also observed in Fig. 9(b) that corresponding to the increase of the draft of the platform, for the platform with the tether–wave interaction being taken into account, the amplitude

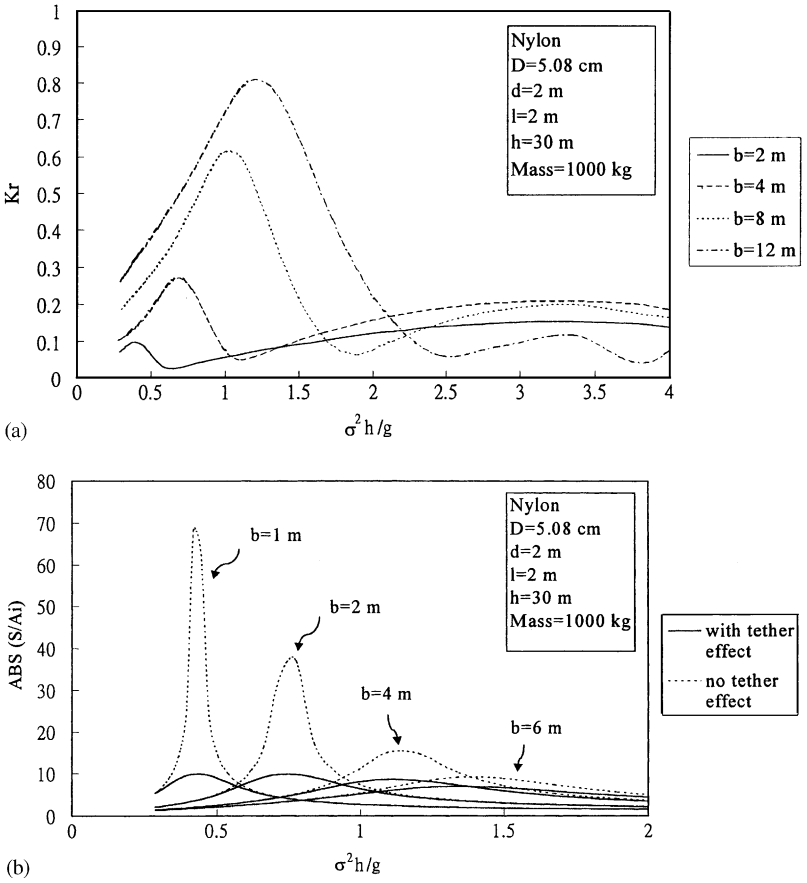

Fig. 8. The dragged surge motion response for the twin-platform system with respect to the variation of platform dimension *b*. (a) The reflection coefficient corresponding to the wave frequency. (b) The motion comparison between the platforms with and without tether–wave interactions.

increased and then dropped slightly after up to a certain value. This phenomenon is quite different from the case where the tether–wave interactions are not considered, where the increase of the platform draft normally enhances the stiffness and thus reduces the platform motion. However, with the consideration of tether–wave interactions, when the tether vibration is larger the damping due to the tether drag will be more effective and thus the reduction on the platform motion is more significant. Once the platform draft increased, corresponding to the reduction of the tether vibration, the damping became less effective and then the tether drag effect became gradually negligible. Therefore, the motion of the platform with deeper draft will be less influenced by the tether–wave interaction, while the motion of platform with smaller draft may be significantly overestimated when this interaction was ignored.

4.2.4. The mass effect on the twin-platform drag surge motion

For the mass variation effect Fig. 10 shows the comparison of dimensionless response amplitude of motions between platforms with and without considering the tether–wave

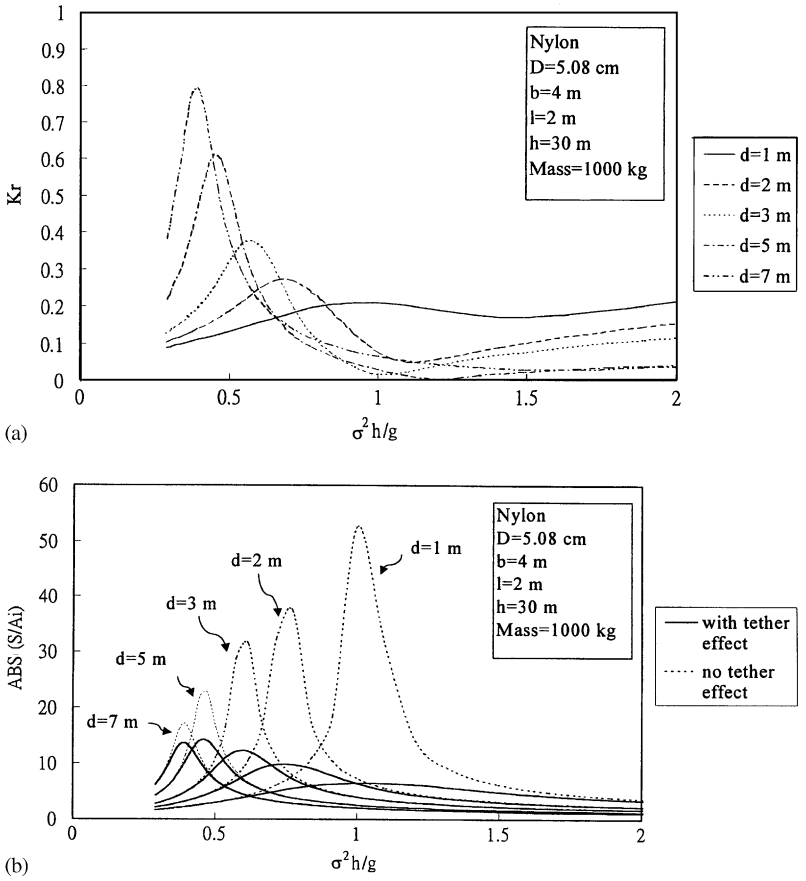

Fig. 9. The dragged surge motion for the twin-platform system with respect to the draft of the platform. (a) The reflection coefficient corresponding to the wave frequency. (b) The motion comparison between the platforms with and without tether–wave interactions.

interactions corresponding to the dimensionless wave frequency. With respect to the increase of the mass, the response amplitude is basically increased, particularly for the case of ignoring the tether–wave interactions, while the resonant frequency moves to the low value range. It is known that the increase of the platform mass will reduce the system frequency and result in the increase of the initial draft, which will reduce the equivalent stiffness and then increase the response magnitude. However, when the tether–wave interaction is taken into consideration, the damping due to tether drag becomes more obvious corresponding to the increase of the structure mass and thus mitigates the mass effect on the amplitude of surge motion.

4.3. Influence of the water depth on the twin-platform motion

The influence of the water depth on the drag surge motion for the twin-platform system was studied and further compared with the motion without tether–wave interactions. A twin-platform

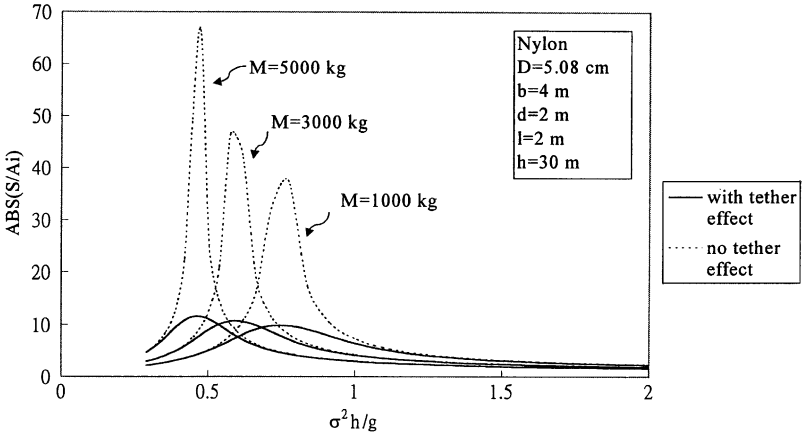

Fig. 10. The comparison for dimensionless amplitude of the surge motion between the platforms with and without tether–wave interactions with respect to the variation of the platform mass.

structural system of 4.0 m dimension for each platform was analyzed when the water depth of the location was varied from 10.0 to 50.0 m. Fig. 11(a) shows the amplitude of the drag surge motion of the platform corresponding to the period of the incident wave and (b) is a comparison between the platform with and without considering the tether–wave interactions. It was found that taking into consideration of the tether–wave interactions, the platform motion was greatly reduced, particularly for locations in the deeper water, and as shown in Fig. 11(a) the water depth seems to influence the resonant period rather than the vibration amplitude. Corresponding to the increase of the water depth, the resonant period of the response was increased for platforms both with and without tether–wave interaction effect. It is clear that, for the platform without considering the tether drag effect, the increase of the water depth would lengthen the tension-leg and then decrease the equivalent stiffness of the system if the dimension and material of the tether remained the same. Once the stiffness of the system reduced, both the amplitude and the resonant period of the response then, increased. However, when the tether–wave interaction was taken into account, the vibration of the lengthened tether would consume more energy input from the waves and thus might reduce the vibration of the platform as was shown in the comparison of Fig. 11(b).

4.4. *Seiching phenomenon for the twin-platform system*

An interesting phenomenon similar to the water oscillations in a basin was observed for the tension-leg twin-platform structural system, where the incident waves reflect in between two platforms of the system. For the scattering problem when the spacing between two platforms is one-half times the incident wavelength, water oscillation occurs between these two platforms. As shown in Fig. 12 the dot-line is the elevation of the water surface near the side face of the platform when the twin-platform structure stays still, where the water oscillates corresponding to $2kl \cong n\pi, n = 1, 2, 3...$ and the spacing of two platforms, $2l$, is about one-half times that of the

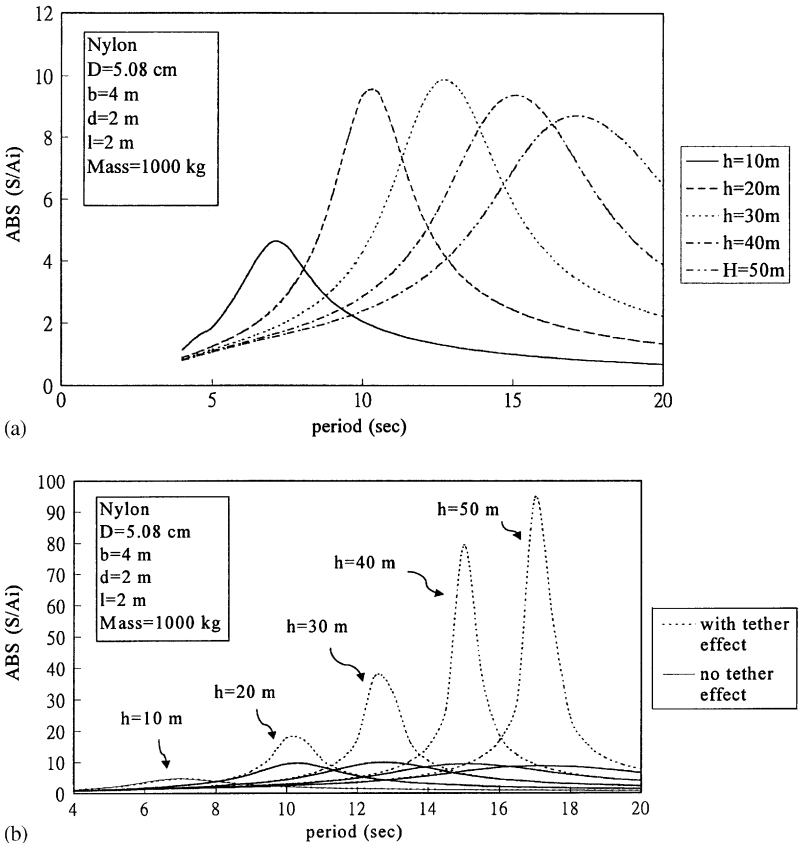

Fig. 11. The dragged surge motion for the twin-platform system with respect to the water depth h. (a) The dimensionless amplitude of the dragged surge motion corresponding to the wave period. (b) The motion comparison between the platforms with and without tether–wave interactions.

wavelength. While a solid line represents the water oscillation when the drag surge motion of the twin platform was taken into account, it shows that the significant peaks of the water oscillation occur around $2kl = n\pi, n = 2, 4, 6....$ It was found that the peaks of water oscillation corresponding to $2kl = n\pi, n = 1, 3, 5...$ become insignificant when these two platforms are in a drag surge motion.

The dimensional effect of the twin-platform system on the water oscillation was further studied. As also shown Fig. 12(a) and (b) shows the water oscillation between two platforms when the dimension of each single platform was varied from 2 to 4 m while the spacing between them remained unchanged. It is found that with respect to the increase of the platform dimension, the oscillation seems to be more significant when $2kl$ is in a lower range for both cases with and without platform motion. However, within a higher range of $2kl$ such that the wavelength is shorter, the water oscillations associated with platform motions seem to be less significant due to the better shielding effect on the short waves for platforms with larger dimensions.

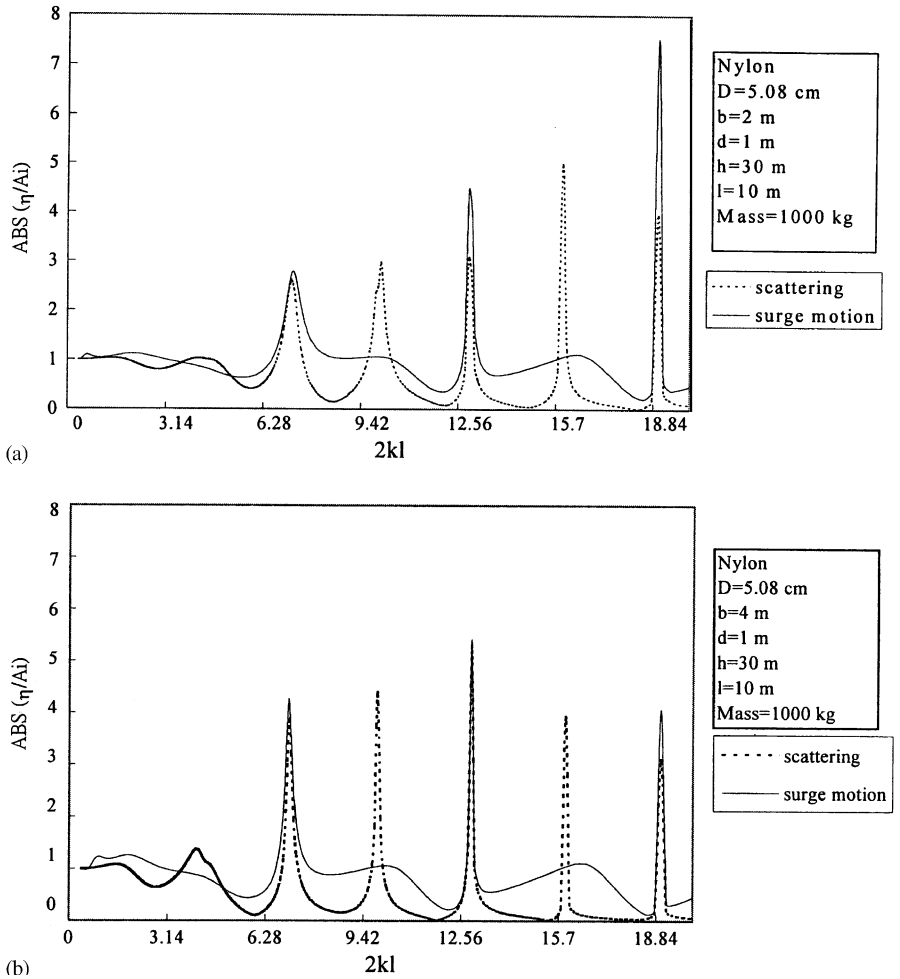

Fig. 12. Comparison of the water oscillations corresponding to $2kl$ with and without considering the drag motion of the platform. (a) The width of each platform is 2 m, (b) 4 m.

5. Conclusions

In this study, a set of equations and corresponding boundary conditions to describe the motion of a twin-platform system with pre-tension tethers subjected to multi-interactions among waves, platform structure and tension-leg tethers were derived. The corresponding analytical solutions of close form were obtained and presented as an infinite series for the dynamic behavior of the platform. The solution was also demonstrated in the numerical examples in terms of the amplitude of the platform surge motion and the reflection and transmission coefficient. The influence from parameters of the structural dimension and the water depth was examined and discussed. As was illustrated in the figures for the analytical results, it is concluded that this analytical solution of infinite series form is convergent and consistent with the single-platform solution.

In the comparisons for the platform responses with and without considering the tether–wave interactions it showed that the tether–wave interactions would significantly reduce the responses in general. However, when the parameters of the platform or wave or water depth varied, the interaction effect was influenced. Among the parameters of twin–platform system, similar to single-platform system, the interaction effect is very significant for platform with small draft or small dimension. The tether–wave interaction effect is also more obvious when the platform mass is larger or when the location of water is deeper. However, when the draft or dimension of the platform is large the interaction effect between the tethers and waves becomes gradually insignificant. The influence of the variation of spacing between two single platforms of a twin-platform system seems to be less significant on the interaction effect than the case without tether–wave interaction. Therefore, it is concluded that for the twin-platform system with smaller dimension or smaller draft or larger mass or platforms located in deeper water, the analysis without taking account for the wave–tether interaction effect tends to overestimate the platform responses no matter what the spacing between two platforms is.

A phenomenon similar to the water oscillations in a basin was also observed for this twin-platform structural system as incident waves reflect in between two platforms of the system. In the scattering problem, the resonant water oscillation occurs when the spacing between two platforms is one-half times the incident wavelength. When the drag surge motion of the twin platform was taken into account it shows that the significant peaks of the water oscillation between platforms occur when the spacing of two platforms is about the multiple times of the wavelength.

Acknowledgements

This study was partially supported by National Science Council, Taiwan under Grant No.88-2611-E-110-008 and is gratefully acknowledged here.

Appendix A

KBC (scattering problem) on $x = -l - b$:

$$\frac{K_\alpha \langle Z_\alpha Z_\alpha \rangle}{\cos K_\alpha h} A_{\mathrm{I}s\alpha} - \mathrm{i}\left[\frac{1}{l+b}\langle Z_{\mathrm{II}1} Z_\alpha \rangle^d A_{\mathrm{II}sP1} + \sum_{j=2}^{\infty} (-1)^{j-1} K_{\mathrm{II}j} Z_{\mathrm{II}j} Z_\alpha^d \times \left(-A_{\mathrm{II}sPj} + \mathrm{e}^{-K_{\mathrm{II}j}(2l+b)} A_{\mathrm{II}sNj}\right)\right] = \delta_{\alpha 1} \mathrm{e}^{K1(l+b)} \frac{K_1 \langle Z_1 Z_1 \rangle}{\cos(K_1 h)} A_i. \tag{A.1}$$

DBC (Scattering Problem) on $x = -l - b$:

$$-\mathrm{i}\sum_{j=1}^{\infty} \frac{\langle Z_{\mathrm{II}\alpha} Z_j \rangle^d}{\cos(K_j h)} A_{\mathrm{I}sj} - \langle Z_{\mathrm{II}\alpha} Z_{\mathrm{II}\alpha} \rangle^d \left\{ \left[(1-\delta_{\alpha 1})(-1)^{\alpha-1} - \delta_{\alpha 1}\right] A_{\mathrm{II}sP\alpha} + \left[(1-\delta_{\alpha 1})(-1)^{\alpha-1} + \delta_{\alpha 1}\right] \mathrm{e}^{-K_{\mathrm{II}\alpha}(2l+b)} A_{\mathrm{II}sN\alpha} \right\} = \mathrm{i}\mathrm{e}^{K_1(l+b)} \frac{\langle Z_{\mathrm{II}\alpha} Z_1 \rangle^d}{\cos(K_1 h)} A_i. \tag{A.2}$$

KBC (scattering problem) on $x = -l$:

$$-\mathrm{i}\frac{\langle Z_{\mathrm{II}1}Z_\alpha\rangle^d}{l+b}A_{\mathrm{II}sP1}-\mathrm{i}\sum_{j=2}^{\infty}\left[(-1)^{j-1}K_{\mathrm{II}j}\langle Z_{\mathrm{II}j}Z_\alpha\rangle^d\left(-\mathrm{e}^{-K_{\mathrm{II}j}b}A_{\mathrm{II}sPj}+\mathrm{e}^{-2K_{\mathrm{II}j}l}A_{\mathrm{II}sNj}\right)\right]+\frac{K_\alpha\langle Z_\alpha Z_\alpha\rangle}{\cos(K_\alpha h)}(-A_{\mathrm{III}sP\alpha}+\mathrm{e}^{-2K_\alpha l}A_{\mathrm{III}sN\alpha})=0. \tag{A.3}$$

DBC (scattering problem) on $x = -l$:

$$\langle Z_{\mathrm{II}\alpha}Z_{\mathrm{II}\alpha}\rangle^d\left\{\left[(1-\delta_{\alpha1})(-1)^{\alpha-1}-\left(l/l+b\right)\delta_{\alpha1}\right]\mathrm{e}^{-K_{\mathrm{II}\alpha}b}A_{\mathrm{II}sP\alpha}+\left[(1-\delta_{\alpha1})(-1)^{\alpha-1}+\delta_{\alpha1}\right]\times\mathrm{e}^{-2K_{\mathrm{II}\alpha}l}A_{\mathrm{II}sN\alpha}\right\}+\mathrm{i}\sum_{j=1}^{\infty}\frac{\langle Z_{\mathrm{II}\alpha}Z_j\rangle^d}{\cos\left(K_jh\right)}\left(A_{\mathrm{III}sPj}+\mathrm{e}^{-2K_jl}A_{\mathrm{III}sNj}\right)=0. \tag{A.4}$$

KBC (scattering problem) on $x = l$:

$$\frac{K_\alpha\langle Z_\alpha Z_\alpha\rangle}{\cos(K_\alpha h)}(-\mathrm{e}^{-2K_\alpha l}A_{\mathrm{III}sP\alpha}+A_{\mathrm{III}sN\alpha})-\mathrm{i}\frac{\langle Z_{\mathrm{II}1}Z_\alpha\rangle^d}{l+b}A_{\mathrm{IV}sP1}-\mathrm{i}\sum_{j=2}^{\infty}\left[(-1)^{j-1}K_{\mathrm{II}j}\langle Z_{\mathrm{II}j}Z_\alpha\rangle^d\left(-\mathrm{e}^{-2K_{\mathrm{II}j}l}A_{\mathrm{IV}sPj}+e^{-K_{\mathrm{ii}j}b}A_{\mathrm{IV}sNj}\right)\right]=0. \tag{A.5}$$

DBC (scattering problem) on $x = l$:

$$\mathrm{i}\sum_{j=1}^{\infty}\frac{\langle Z_{\mathrm{II}\alpha}Z_j\rangle^d}{\cos\left(K_jh\right)}\left(\mathrm{e}^{-2K_jl}A_{\mathrm{III}sPj}+A_{\mathrm{III}sNj}\right)+\langle Z_{\mathrm{II}\alpha}Z_{\mathrm{II}\alpha}\rangle^d\left\{\left[(1-\delta_{\alpha1})(-1)^{\alpha-1}+\left(l/l+b\right)\delta_{\alpha1}\right]\times\mathrm{e}^{-2K_{\mathrm{II}\alpha}l}A_{\mathrm{IV}sP\alpha}+\left[(1-\delta_{\alpha1})(-1)^{\alpha-1}+\delta_{\alpha1}\right]e^{-K_{\mathrm{II}\alpha}b}A_{\mathrm{IV}sN\alpha}\right\}=0. \tag{A.6}$$

KBC (scattering problem) on $x = l + b$:

$$\mathrm{i}\frac{\langle Z_{\mathrm{II}1}Z_\alpha\rangle^d}{l+b}A_{\mathrm{IV}sP1}+\mathrm{i}\sum_{j=2}^{\infty}\left[(-1)^{j-1}K_{\mathrm{II}j}\langle Z_{\mathrm{II}j}Z_\alpha\rangle^d\left(-\mathrm{e}^{-K_{\mathrm{II}j}(2l+b)}A_{\mathrm{IV}sPj}+A_{\mathrm{IV}sNj}\right)\right]+\frac{K_\alpha\langle Z_\alpha Z_\alpha\rangle}{\cos(K_\alpha h)}A_{\mathrm{V}s\alpha}=0. \tag{A.7}$$

DBC (scattering problem) on $x = l + b$:

$$\langle Z_{\mathrm{II}\alpha}Z_{\mathrm{II}\alpha}\rangle^d\left\{\left[(1-\delta_{\alpha1})(-1)^{\alpha-1}+\delta_{\alpha1}\right]\mathrm{e}^{-K_{\mathrm{II}\alpha}(2l+b)}A_{\mathrm{IV}sP\alpha}+\left[(1-\delta_{\alpha1})(-1)^{\alpha-1}+\delta_{\alpha1}\right]A_{\mathrm{IV}sN\alpha}\right\}+\mathrm{i}\sum_{j=1}^{\infty}\frac{\langle Z_{\mathrm{II}\alpha}Z_j\rangle^d}{\cos\left(K_jh\right)}A_{\mathrm{V}sj}=0, \tag{A.8}$$

where δ is the Kronecker delta and notations $\langle Z_\bullet Z_\bullet\rangle^\bullet$ are defined as Eqs. (D.1)–(D.3) in Appendix D.

KBC (radiation problem) on $x = -l - b$:

$$\frac{K_\alpha\langle Z_\alpha Z_\alpha\rangle}{\cos K_\alpha h}A_{\mathrm{I}w\alpha} - \mathrm{i}\frac{1}{l+b}\langle Z_{\mathrm{II}1}Z_\alpha\rangle^d A_{\mathrm{II}wP1} - \mathrm{i}\sum_{j=2}^{\infty}\Big[(-1)^{j-1}K_{\mathrm{II}j}\big\langle Z_{\mathrm{II}j}Z_\alpha\big\rangle^d\big(-A_{\mathrm{II}wPj} + \mathrm{e}^{-K_{\mathrm{II}j}(2l+b)}A_{\mathrm{II}wNj}\big)\Big] - \frac{\mathrm{i}\sigma^2}{g}\langle Z_\alpha^0\rangle S = 0. \tag{A.9}$$

DBC (radiation problem) on $x = -l - b$:

$$-\mathrm{i}\sum_{j=1}^{\infty}\frac{\big\langle Z_{\mathrm{II}\alpha}Z_j\big\rangle^d}{\cos\big(K_j h\big)}A_{\mathrm{I}wj} - \langle Z_{\mathrm{II}\alpha}Z_{\mathrm{II}\alpha}\rangle^d\big\{\big[(1-\delta_{\alpha1})(-1)^{\alpha-1} - \delta_{\alpha1}\big]A_{\mathrm{II}wP\alpha} + \big[(1-\delta_{\alpha1})(-1)^{\alpha-1} + \delta_{\alpha1}\big]\mathrm{e}^{-K_{\mathrm{II}\alpha}(2l+b)}A_{\mathrm{II}wN\alpha}\big\} = 0. \tag{A.10}$$

KBC (radiation problem) on $x = -l$:

$$-\mathrm{i}\frac{\langle Z_{\mathrm{II}1}Z_\alpha\rangle^d}{l+b}A_{\mathrm{II}wP1} - \mathrm{i}\sum_{j=2}^{\infty}\big[(-1)^{j-1}K_{\mathrm{II}j}\big\langle Z_{\mathrm{II}j}Z_\alpha\big\rangle^d\big(-\mathrm{e}^{-K_{\mathrm{II}j}b}A_{\mathrm{II}wPj} + \mathrm{e}^{-2K_{\mathrm{II}j}l}A_{\mathrm{II}wNj}\big)\big] + \frac{K_\alpha\langle Z_\alpha Z_\alpha\rangle}{\cos(K_\alpha h)}\big(-A_{\mathrm{III}w\alpha} + \mathrm{e}^{-2K_\alpha l}A_{\mathrm{III}wN\alpha}\big) - \frac{\mathrm{i}\sigma^2}{g}\langle Z_\alpha^0\rangle S = 0. \tag{A.11}$$

DBC (radiation problem) on $x = -l$:

$$\langle Z_{\mathrm{II}\alpha}Z_{\mathrm{II}\alpha}\rangle^d\mathrm{e}^{-K_{\mathrm{II}\alpha}b}A_{\mathrm{II}wP\alpha} + \big\{\big[(1-\delta_{\alpha1})(-1)^{\alpha-1} - \big(l/l+b\big)\delta_{\alpha1}\big]\mathrm{e}^{-K_{\mathrm{II}\alpha}b}A_{\mathrm{II}wP\alpha} + \big[(1-\delta_{\alpha1})(-1)^{\alpha-1} + \delta_{\alpha1}\big]\mathrm{e}^{-2K_{\mathrm{II}\alpha}l}A_{\mathrm{II}wN\alpha}\big\} + \mathrm{i}\sum_{j=1}^{\infty}\frac{\big\langle Z_{\mathrm{II}\alpha}Z_j\big\rangle^d}{\cos\big(K_j h\big)}\big(A_{\mathrm{III}wPj} + \mathrm{e}^{-2K_j l}A_{\mathrm{III}wNj}\big) = 0. \tag{A.12}$$

KBC (radiation problem) on $x = l$:

$$\frac{K_\alpha\langle Z_\alpha Z_\alpha\rangle}{\cos(K_\alpha h)}\big(-\mathrm{e}^{-2K_\alpha l}A_{\mathrm{III}wP\alpha} + A_{\mathrm{III}wN\alpha}\big) - \mathrm{i}\frac{\langle Z_{\mathrm{II}1}Z_\alpha\rangle^d}{l+b}A_{\mathrm{II}wP1} - \mathrm{i}\sum_{j=2}^{\infty}\Big[(-1)^{j-1}K_{\mathrm{II}j}\big\langle Z_{\mathrm{II}j}Z_\alpha\big\rangle^d\big(-\mathrm{e}^{-2K_{\mathrm{II}j}l}A_{\mathrm{IV}wPj} + \mathrm{e}^{-K_{\mathrm{II}j}b}A_{\mathrm{IV}wNj}\big)\Big] - \frac{\mathrm{i}\sigma^2}{g}\langle Z_\alpha^0\rangle S = 0. \tag{A.13}$$

DBC (radiation problem) on $x = l$:

$$\mathrm{i}\sum_{j=1}^{\infty}\frac{\big\langle Z_{\mathrm{II}\alpha}Z_j\big\rangle^d}{\cos(K_j h)}\big(\mathrm{e}^{-2K_j l}A_{\mathrm{III}wPj} + A_{\mathrm{III}wNj}\big) + \langle Z_{\mathrm{II}\alpha}Z_{\mathrm{II}\alpha}\rangle^d\big\{\big[(1-\delta_{\alpha1})(-1)^{\alpha-1} + \big(l/l+2b\big)\delta_{\alpha1}\big] \times \mathrm{e}^{-2K_{\mathrm{II}\alpha}l}A_{\mathrm{IV}wP\alpha} + \big[(1-\delta_{\alpha1})(-1)^{\alpha-1} + \delta_{\alpha1}\big]\mathrm{e}^{-K_{\mathrm{II}\alpha}b}A_{\mathrm{IV}wN_\alpha}\big\} = 0. \tag{A.14}$$

KBC (radiation problem) on $x = l + b$:

$$\mathrm{i}\frac{\langle Z_{\mathrm{II}1}Z_\alpha\rangle^d}{l+b}A_{\mathrm{IV}wP1} + \mathrm{i}\sum_{j=2}^{\infty}\big[(-1)^{j-1}K_{\mathrm{II}j}\big\langle Z_{\mathrm{II}j}Z_\alpha\big\rangle^d\big(-\mathrm{e}^{-K_{\mathrm{II}j}(2l+b)}A_{\mathrm{IV}wPj} + A_{\mathrm{IV}wNj}\big)\big] + \frac{K_\alpha\langle Z_\alpha Z_\alpha\rangle}{\cos(K_\alpha h)}A_{\mathrm{V}w\alpha} + \frac{\mathrm{i}\sigma^2}{g}\langle Z_\alpha^0\rangle S = 0. \tag{A.15}$$

DBC (radiation problem) on $x = l + b$:

$$\langle Z_{\mathrm{II}\alpha} Z_{\mathrm{II}\alpha}\rangle^{d}\left\{\left[(1-\delta_{\alpha 1})(-1)^{\alpha-1}+\delta_{\alpha 1}\right]\mathrm{e}^{-K_{\mathrm{II}\alpha}(2l+b)}A_{\mathrm{IV}wP\alpha}\right.$$
$$\left.+\left[(1-\delta_{\alpha 1})(-1)^{\alpha-1}+\delta_{\alpha 1}\right]A_{\mathrm{IV}wN\alpha}+\mathrm{i}\sum_{j=1}^{\infty}\frac{\langle Z_{\mathrm{II}\alpha}Z_j\rangle^{d}}{\cos(K_j h)}A_{\mathrm{V}wj}=0, \tag{A.16}$$

where again the notations of $\left\langle Z_j^0\right\rangle$ and $\langle Z_\bullet Z_\bullet\rangle^\bullet$ are defined in Appendix D.

Appendix B

$$a=\pm\sqrt{-\frac{1}{T^*}\left\{\sigma^2\left[\rho^*+0.25\pi\rho_w D^2(C_m-1)\right]+\mathrm{i}\sigma(C+R_{d1}^{**}\rho_w D\sigma)\right\}}, \tag{B.1}$$

$$a^*=\pm\sqrt{-\frac{1}{T^*}\left\{\sigma^2\left[\rho^*+0.25\pi\rho_w D^2(C_m-1)\right]+\mathrm{i}\sigma(C+R_{d2}^{**}\rho_w D\sigma)\right\}}, \tag{B.2}$$

$$C_1=\frac{1}{\mathrm{e}^{a(h-d)}-\mathrm{e}^{-a(h-d)}}\left\{\mathrm{e}^{ah}\left[S-\sum_{n=1}^{\infty}a_n\cos K_{\mathrm{II}n}(h-d)\right]+\mathrm{e}^{ad}\sum_{n=1}^{\infty}a_n\right\}, \tag{B.3}$$

$$C_1^*=\frac{1}{\mathrm{e}^{a^*(h-d)}-\mathrm{e}^{-a^*(h-d)}}\left\{\mathrm{e}^{a^*h}\left[S-\sum_{n=1}^{\infty}a_n^*\cos K_{\mathrm{II}n}(h-d)\right]+\mathrm{e}^{a^*d}\sum_{n=1}^{\infty}a_n^*\right\}, \tag{B.4}$$

$$C_2=\frac{1}{\mathrm{e}^{a(h-d)}-\mathrm{e}^{-a(h-d)}}\left\{\mathrm{e}^{-ah}\left[\sum_{n=1}^{\infty}a_n\cos K_{\mathrm{II}n}(h-d)-S\right]-\mathrm{e}^{-ad}\sum_{n=1}^{\infty}a_n\right\}, \tag{B.5}$$

$$C_2^*=\frac{1}{\mathrm{e}^{a^*(h-d)}-\mathrm{e}^{-a^*(h-d)}}\left\{\mathrm{e}^{-a^*h}\left[\sum_{n=1}^{\infty}a_n^*\cos K_{IIn}(h-d)-S\right]-\mathrm{e}^{-a^*d}\sum_{n=1}^{\infty}a_n^*\right\}, \tag{B.6}$$

$$a_1=\frac{A_{\mathrm{II}s/wP1}(0.25\pi\rho_w C_m D^2 g+\mathrm{i}\rho_w D R_{d1}^{**}g)}{(l+b)\left\{\sigma^2\left[\rho^*+0.25\pi\rho_w D^2(C_m-1)\right]+\mathrm{i}\sigma(C+R_{d1}^{**}\rho_w D\sigma)\right\}}, \tag{B.7}$$

$$a_1^*=\frac{A_{\mathrm{IV}s/wP1}(0.25\pi\rho_w C_m D^2 g+\mathrm{i}\rho_w D R_{d2}^{**}g)}{(l+b)\left\{\sigma^2\left[\rho^*+0.25\pi\rho_w D^2(C_m-1)\right]+\mathrm{i}\sigma(C+R_{d2}^{**}\rho_w D\sigma)\right\}}, \tag{B.8}$$

$$a_n = \frac{1}{-T^*(K_{\mathrm{II}n})^2 + \sigma^2\left[\rho^* + 0.25\pi\rho_w D^2(C_m - 1)\right] + \mathrm{i}\sigma\left(C + R_{d1}^{**}\rho_w D\sigma\right)} \times (0.25\pi\rho_w D^2 C_m g + \mathrm{i}\rho_w D R_{d1}^{**} g)(-1)^{n-1}\left[-K_{\mathrm{II}n}A_{\mathrm{II}s/wPn}\mathrm{e}^{-(x_1+l+b)K_{\mathrm{II}n}} + K_{\mathrm{II}n}A_{\mathrm{II}s/wNn}\mathrm{e}^{(x_1-l)K_{\mathrm{II}n}}\right], \quad n \geqslant 2 \tag{B.9}$$

$$a_n^* = \frac{1}{-T^*(K_{\mathrm{II}n})^2 + \sigma^2\left[\rho^* + 0.25\pi\rho_w D^2(C_m - 1)\right] + \mathrm{i}\sigma\left(C + R_{d2}^{**}\rho_w D\sigma\right)} \times (0.25\pi\rho_w D^2 C_m g + \mathrm{i}\rho_w D R_{d2}^{**} g)(-1)^{n-1}\left[-K_{\mathrm{II}n}A_{\mathrm{IV}s/wPn}\mathrm{e}^{-(x_2+l)K_{\mathrm{II}n}} + K_{\mathrm{II}n}A_{\mathrm{IV}s/wNn}\mathrm{e}^{(x_2-l-b)K_{\mathrm{II}n}}\right], \quad n \geqslant 2 \tag{B.10}$$

Appendix C

$$\lambda_1 = \frac{C_1}{a}\left(\mathrm{e}^{-ad} - \mathrm{e}^{-ah}\right) + \frac{-C_2}{a}\left(\mathrm{e}^{ad} - \mathrm{e}^{ah}\right) + \sum_{n=1}^{\infty}\frac{a_n}{K_{\mathrm{II}n}}\sin K_{\mathrm{II}n}(h-d), \tag{C.1}$$

$$\lambda_2 = \frac{C_1^*}{a^*}\left(\mathrm{e}^{-a^*d} - \mathrm{e}^{-a^*h}\right) + \frac{-C_2^*}{a^*}\left(\mathrm{e}^{a^*d} - \mathrm{e}^{a^*h}\right) + \sum_{n=1}^{\infty}\frac{a_n^*}{K_{\mathrm{II}n}}\sin K_{\mathrm{II}n}(h-d), \tag{C.2}$$

$$\beta = \rho_w D\sigma^2\left[0.25\pi D(C_m - 1) + \mathrm{i}R_{d1}^*\right], \tag{C.3}$$

$$\beta^* = \rho_w D\sigma^2\left[0.25\pi D(C_m - 1) + \mathrm{i}R_{d2}^*\right], \tag{C.4}$$

$$Q = \frac{\mathrm{e}^{a(d-h)} + \mathrm{e}^{-a(d-h)} - 2}{a[\mathrm{e}^{a(h-d)} - \mathrm{e}^{-a(h-d)}]}, \tag{C.5}$$

$$Q^* = \frac{\mathrm{e}^{a^*(d-h)} + \mathrm{e}^{-a^*(d-h)} - 2}{a^*[\mathrm{e}^{a^*(h-d)} - \mathrm{e}^{-a^*(h-d)}]}, \tag{C.6}$$

$$\begin{aligned}\Gamma_n = {} & \frac{\mathrm{e}^{-ad} - \mathrm{e}^{-ah}}{a}\frac{1}{v}\left[-\mathrm{e}^{ah}\varsigma_n\cos[K_{\mathrm{II}n}(h-d)] + \mathrm{e}^{ad}\varsigma_n\right] \\ & + \frac{-\left(\mathrm{e}^{ad} - \mathrm{e}^{ah}\right)}{a}\frac{1}{v}\left[\mathrm{e}^{-ah}\varsigma_n\cos[K_{\mathrm{II}n}(h-d)] - \mathrm{e}^{-ad}\varsigma_n\right] + \frac{\sin[K_{\mathrm{II}n}(h-d)]}{K_{\mathrm{II}n}}\varsigma_n,\end{aligned} \tag{C.7}$$

$$\begin{aligned}\Gamma_n^* = {} & \frac{\mathrm{e}^{-a^*d} - \mathrm{e}^{-a^*h}}{a^*}\frac{1}{v^*}\left[-\mathrm{e}^{a^*h}\varsigma_n^*\cos[K_{\mathrm{II}n}(h-d)] + \mathrm{e}^{a^*d}\varsigma_n^*\right] \\ & + \frac{-\left(\mathrm{e}^{a^*d} - \mathrm{e}^{a^*h}\right)}{a^*}\frac{1}{v^*}\left[\mathrm{e}^{-a^*h}\varsigma_n^*\cos[K_{\mathrm{II}n}(h-d)] - \mathrm{e}^{-a^*d}\varsigma_n^*\right] \\ & + \frac{\sin[K_{\mathrm{II}n}(h-d)]}{K_{\mathrm{II}n}}\varsigma_n^*, \quad n \geqslant 2\end{aligned} \tag{C.8}$$

where

$$v = e^{a(h-d)} - e^{-a(h-d)}, \quad v^* = e^{a^*(h-d)} - e^{-a^*(h-d)},$$

$$\varsigma_n = \frac{(-1)^{n-1}\left[0.25\pi\rho_W D^2 C_m g + i\rho_w D R^*_{d1} g\right](K_{IIn})}{-T^*(K_{IIn})^2 + \sigma^2\left[\rho^* + 0.25\pi\rho_w D^2(C_m - 1)\right] + i\sigma\left(C + R^*_{d1}\rho_w D\sigma\right)}, \quad n \geqslant 2$$

and

$$\varsigma^*_n = \frac{(-1)^{n-1}\left[0.25\pi\rho_W D^2 C_m g + i\rho_w D R^*_{d2} g\right](K_{IIn})}{-T^*(K_{IIn})^2 + \sigma^2\left[\rho^* + 0.25\pi\rho_w D^2(C_m - 1)\right] + i\sigma\left(C + R^*_{d2}\rho_w D\sigma\right)}, \quad n \geqslant 2,$$

$$\begin{aligned}\varsigma_1 = &\frac{\left[0.25\pi\rho_W D^2 C_m g + i\rho_w D R^*_{d1} g\right]\cos[K_{II1}(h-d)]}{avb\sigma^2\left[\rho^* + 0.25\pi\rho_w D^2(C_m - 1)\right] + i\sigma\left(C + R^*_{d1}\rho_w D\sigma\right)}\left[2 - e^{a(h-d)} - e^{a(d-h)}\right] \\ &+ \frac{\left[0.25\pi\rho_W D^2 C_m g + i\rho_w D R^*_{d1} g\right]}{avb\sigma^2\left[\rho^* + 0.25\pi\rho_w D^2(C_m - 1)\right] + i\sigma\left(C + R^*_{d1}\rho_w D\sigma\right)}\left[2 - e^{a(d-h)} - e^{a(h-d)}\right], \quad \text{(C.9)}\end{aligned}$$

$$\begin{aligned}\varsigma^*_1 = &\frac{\left[0.25\pi\rho_W D^2 C_m g + i\rho_w D R^*_{d2} g\right]\cos[K_{II1}(h-d)]}{a^* v^* b\sigma^2\left[\rho^* + 0.25\pi\rho_w D^2(C_m - 1)\right] + i\sigma\left(C + R^*_{d2}\rho_w D\sigma\right)}\left[2 - e^{a^*(h-d)} - e^{a^*(d-h)}\right] \\ &+ \frac{\left[0.25\pi\rho_W D^2 C_m g + i\rho_w D R^*_{d2} g\right]}{a^* v^* b\sigma^2\left[\rho^* + 0.25\pi\rho_w D^2(C_m - 1)\right] + i\sigma\left(C + R^*_{d2}\rho_w D\sigma\right)}\left[2 - e^{a^*(d-h)} - e^{a^*(h-d)}\right], \quad \text{(C.10)}\end{aligned}$$

$$G_n = \rho_w D\sigma R_{d1}(-1)^{n-1}\sin[K_{IIn}(h-d)]ig/\sigma, \quad \text{(C.11)}$$

$$G^*_n = \rho_w D\sigma R_{d2}(-1)^{n-1}\sin[K_{IIn}(h-d)]ig/\sigma, \quad n \geqslant 2. \quad \text{(C.12)}$$

Appendix D

$$\begin{aligned}\langle Z_j Z_\alpha \rangle &= \int_{-h}^{0} \cos\left[K_j(z+h)\right]\cos[K_\alpha(z+h)]\,dz \\ &= \begin{cases} 0 & \text{if } j \neq \alpha, \\ \dfrac{h}{2}\left[1 + \dfrac{\sinh(2K_\alpha h)}{2K_\alpha h}\right] & \text{if } j = \alpha, \end{cases} \quad \text{(D.1)}\end{aligned}$$

$$\langle Z_{\mathrm{II}j} Z_\alpha \rangle^d = \int_{-h}^{-d} \cos\big[K_{\mathrm{II}j}(z+h)\big]\cos[K_\alpha(z+h)]\,\mathrm{d}z$$
$$= \begin{cases} \dfrac{h-d}{2}\left\{1+\dfrac{\sin[2K_\alpha(h-d)]}{2K_\alpha h}\right\}, & \text{if } K_{\mathrm{II}j}=K_\alpha, \\ \dfrac{1}{2}\left\{\dfrac{\sin\big[(K_{\mathrm{II}j}+K_\alpha)(h-d)\big]}{K_{\mathrm{II}j}+K_\alpha}+\dfrac{\sin\big[(K_{\mathrm{II}j}-K_\alpha)(h-d)\big]}{K_{\mathrm{II}j}-K_\alpha}\right\} & \text{if } K_{\mathrm{II}j}\neq K_\alpha, \end{cases} \tag{D.2}$$

$$\langle Z_{\mathrm{II}j} Z_{\mathrm{II}\alpha} \rangle^d = \int_{-h}^{-d} \cos\big[K_{\mathrm{II}j}(z+h)\big]\cos[K_{\mathrm{II}\alpha}(z+h)]\,\mathrm{d}z$$
$$= \begin{cases} 0 & \text{if } j\neq\alpha, \\ h-d & \text{if } j=\alpha=1, \\ \dfrac{h-d}{2} & \text{if } j=\alpha\neq 1, \end{cases} \tag{D.3}$$

$$\left\langle Z_j^0 \right\rangle = \int_{-d}^{0} \cos\big[K_j(z+h)\big]\,\mathrm{d}z = \frac{1}{K_j}\big[\sin K_j h - \sin K_j(h-d)\big] \tag{D.4}$$

References

[1] C.J. Garrison, Dynamic response of floating bodies, OTC 2067 (1974) 365–378.
[2] T. Sarpkaya, M. Isaacson, Mechanics of Wave Forces on Offshore Structures, Van Nostrand Reinhold, New York, 1981.
[3] C.C. Mei, Numerical methods in water wave diffraction and radiation, Annual Reviews in Fluid Mechanics 10 (1978) 393.
[4] T. Yamamoto, A. Yoshida, T. Ijima, Dynamics of elastically moored floating objects, in: C.L. Kirk (Ed.), Dynamics Analysis of Offshore Structures, CML, Southampton, 1982.
[5] C.-P. Lee, J.-F. Lee, Wave induced surge motion of a tension leg structure, Ocean Engineering 20 (20) (1993) 171–186.
[6] H.H. Lee, P.-W. Wang, C.-P. Lee, Dragged surge motion of tension leg platforms and strained elastic tethers, Ocean Engineering 26 (1999) 579–594.
[7] H.H. Lee, P.-W. Wang, Analytical solution on the surge motion of tension leg twin platform structural systems, Ocean Engineering 27 (2000) 393–415.
[8] H.H. Lee, W.-S. Wang, Analytical solution on the dragged surge vibration of TLPs with wave large body and small body multi-interactions, Journal of Sound and Vibration 248 (2001) 533–556.
[9] J.L. Black, C.C. Mei, M.C.G. Bray, Radiation and scattering of water waves by rigid bodies, Journal of Fluid Mechanics 46 (1971) 151–164.
[10] J.N. Newman, Marine Hydrodynamics, MIT Press, Cambridge, MA, 1981.
[11] C.K. Solliitt, R.H. Cross, Wave transmission through permeable breakwaters, Proceeding of the 13th ICCE, ASCE, 1972.